Journal of Computational Physics **162,** 186–218 (2000)
doi:10.1006/jcph.2000.6532, available online at http://www.idealibrary.com on IDEAL®

Numerical Approach to Fast Reactions in Reaction-Diffusion Systems: Application to Buffered Calcium Waves in Bistable Models

Boris M. Slepchenko,* James C. Schaff,* and Y. S. Choi†

*Center for Biomedical Imaging Technology, Department of Physiology, University of Connecticut Health Center, Farmington, Connecticut 06030; †Department of Mathematics, University of Connecticut, Storrs, Connecticut 06269.
E-mail: boris@photon.uchc.edu, schaff@panda.uchc.edu, choi@math.uconn.edu

Received January 5, 2000; revised May 1, 2000

A numerical approach to modeling a biochemical system that includes processes with significantly different time scales has been developed within the Virtual Cell environment (J. Schaff *et al.*, 1997, *Biophys. J.* **73**, 1135). The key features of the algorithm are time splitting of slow and fast processes and pseudo-steady approximation based on stoichiometry analysis. We apply the method to study the effect of fast calcium buffering on the properties of self-sustaining calcium waves in living cells. Numerical results for one-dimensional traveling waves in one-variable bistable models are compared with theoretical predictions. The effect of a mobile buffer on calcium waves appears to strongly depend on buffer affinity and system excitability. In systems with low excitability, the buffer can stop the traveling wave and make it move in the opposite direction, which means physiologically that the wave becomes self-extinguishing. We then consider traveling waves in a more realistic two-variable model (the Li–Rinzel model). This system exhibits a new feature: in the mode of low excitability, under certain conditions, it undergoes bifurcation with the buffer concentration as a bifurcation parameter. As a consequence, for some buffer concentrations, there exist two stable traveling waves with very different velocities. Finally, to study how a fluorescent indicator, which acts as a mobile buffer, might affect the fertilization calcium waves in eggs, we run three-dimensional simulations within the Li–Rinzel model using realistic parameters, geometry, and initial conditions. The results indicate strong interaction of a fluorescent dye with initiating calcium spikes. As a result, a fluorescent dye added to visualize calcium dynamics in a cell causes a delay in wave formation and, at sufficient concentration, can prevent a wave.

Key Words: cell modeling; reaction-diffusion systems; pseudo-steady approximation; calcium buffering; bistability; Li–Rinzel model.

0021-9991/00 $35.00

1. INTRODUCTION AND BIOLOGICAL BACKGROUND

A general computational framework for modeling cell biochemical processes, the "Virtual Cell," is being developed at the National Resource for Cell Analysis and Modeling at the University of Connecticut Health Center [1, 2]. It is intended to be a tool for experimentalists (as well as theorists) to test their hypotheses and models. Models are constructed from biochemical and electrophysiological data mapped to appropriate subcellular domains in images obtained from a microscope. Chemical kinetics, membrane fluxes, and diffusion are thus coupled and the resultant reaction-diffusion equations with specified membrane jump conditions and boundary conditions are solved numerically within the given one-, two-, or three-dimensional domains. The results are mapped back to experimental images and can be analyzed by applying the arsenal of image processing tools that is familiar to a cell biologist.

It is generally true that a biological process will be composed of a set of events with vastly different time scales. Unless special precautions are taken in numerical calculations, the fast events will necessitate a small time step for their resolution, in order to avoid numerical instability. Since the total time for the slow processes to finish is very long, this makes the computations expensive. Thus, one has to address this issue when developing a general-purpose tool for cell modeling. We first faced this problem when we applied the Virtual Cell to modeling calcium dynamics in neuroblastoma cells [3, 4]. In this case, calcium buffering—the calcium interaction with molecular species that have calcium binding sites—is thought to be a much faster process than the other key elements, calcium diffusion and fluxes from (and back to) the internal calcium stores. In 1994 Wagner and Keizer developed the rapid buffer approximation to deal with this problem [5]. They used a pseudo-steady approximation to exclude "fast variables" and derived an effective transport equation for calcium. This equation, in general, is no longer of a reaction-diffusion type. Thus, we could not use this approach in our general framework directly because (1) it would require a user to do preliminary analytical work, which can often be quite involved, and, more importantly, (2) in each particular case the final equations might be of different forms and require different algorithms. What we need is a general, purely numerical, approach that can be applied to any reaction-diffusion system with fast subsystems, no matter how complex its reaction scheme is.

We have developed such an approach using the well-known idea of time splitting [6]. In our case, time splitting involves updating variables in two steps, separately for slow processes and for fast reactions. Thus, we always remain within a general reaction-diffusion scheme. In the current approach, to update variables in fast reactions, we use a pseudo-steady approximation; i.e., we replace ordinary differential equations with algebraic equations that reflect rapid equilibrium of fast reactions. At this point care must be taken in choosing a number of independent algebraic equations equal to the number of unknowns. This is achieved with stoichiometry analysis [7, 8] that results in a coupled system of nonlinear algebraic equations and a set of linear constraints, corresponding to conservation relationships within the fast subsystem. It is important that the values of "fast" invariants are updated at each time step using results from solving "slow" equations. The stoichiometry analysis is performed automatically within our framework after a user specifies which reactions are considered fast. After the system of nonlinear equations is determined, we use Newton iterations to solve it. Solutions from the previous time step serve as a good initial guess and ensure rapid convergence of iterations. Symbolic differentiation is automatically invoked to determine the Jacobian matrix of the nonlinear system.

The pseudo-steady approximation has its scope of applicability, as illustrated by the example in Section 2. Obviously, it gives accurate results if the ratio of characteristic times of fast and slow processes τ_{fast}/τ_{slow} is sufficiently small during the transient. In fact, our results indicate that the relative error introduced by the approximation is roughly of the order of τ_{fast}/τ_{slow}. However, in nonlinear systems this ratio may vary in the process and therefore the inequality $\tau_{fast}/\tau_{slow} \ll 1$ might be violated. In formal singular perturbation language, there might be interior layers in the solutions with rapid change of variables. In case one would like to resolve the interior layers, more accurate approaches should be used. We still can take advantage of time splitting because it allows us to decouple fast and slow parts of a system and apply different techniques for their treatment. Staying within this framework, we can now treat the reaction terms with a stiff solver instead of pseudo-steady approximation. Still, in many practical applications the species concentrations do not change rapidly after the initial fast transient, and the pseudo-steady approximation works well. One of the practical conveniences of the pseudo-steady approximation is that it does not require the values of kinetic constants of fast reactions. All that is required are equilibrium constants which are usually available from experimental data.

In this paper we apply our approach to study the effect of fast mobile buffers on calcium waves in bistable systems. Calcium oscillations and waves play an important role as a prerequisite for triggering various physiological processes such as hormone secretion, cell division, muscle contraction, etc. [9]. One of the key elements of intracellular calcium dynamics is calcium release from the endoplasmic reticulum (ER), the internal calcium store, through calcium channels that can be activated by cytoplasmic calcium as well as by other signaling molecules that are present in the cytoplasm, such as inositol-1,4,5-triphosphate ($InsP_3$). Two other components of the calcium flux across the ER membrane are direct leak through the membrane and calcium uptake by molecular pumps—the proteins embedded in the membranes that pump calcium ions back into the ER against its gradient (of course, to do that, they consume energy). The calcium concentration in ER is several orders of magnitude higher than that in the cytoplasm; therefore, for many purposes the store can be considered to have infinite capacity. ER has very complex irregular geometry [10]. Being a continuous closed compartment, it fills a cell with generally non-uniform density while occupying only approximately 15% of the cell volume. In a continuous approximation, it can be modeled by calcium sources and sinks continuously distributed with a certain density throughout a cell and characterized by certain rates. When combined with calcium diffusion, they give rise to a reaction-diffusion type equation [11]

$$\frac{\partial c}{\partial t} = D_c \nabla^2 c + f, \tag{1.1}$$

where c is the calcium concentration, D_c is the calcium diffusion coefficient, and $f = J_{channel} + J_{pump} + J_{leak}$ is the rate of change of calcium concentration due to fluxes through calcium channels, pumps, and because of leak. Calcium fluxes across the outer membrane may also influence calcium dynamics and can be taken into account through the appropriate boundary conditions.

Calcium buffering is another factor which is now widely recognized to have a strong impact on the overall intracellular calcium dynamics [12, 13]. Consider the case of a single mobile buffer interacting with calcium according to the reaction

$$Ca + B \rightleftharpoons CaB, \tag{1.2}$$

where B and CaB denote the free and bound forms of the buffer, respectively. Assuming zero flux boundary conditions for the buffer, same diffusion coefficients for both forms of the buffer, and the total buffer concentration $b_t = [B] + [CaB]$ being spatially uniform initially, b_t is then conserved at each spatial point for any $t > 0$. Here, $[B]$ and $[CaB]$ are the concentrations of the free and bound forms of the buffer, respectively. This system is described by the set of equations

$$\begin{aligned} \frac{\partial c}{\partial t} &= D_c \nabla^2 c + f + R, \\ \frac{\partial b}{\partial t} &= D_b \nabla^2 b - R, \\ R &= -k_{on} c(b_t - b) + k_{off} b, \end{aligned} \tag{1.3}$$

where $b = [CaB]$, D_b is the buffer diffusion coefficient, and k_{on} and k_{off} are the reaction kinetic constants. As we mentioned above, calcium buffering is considered to be much faster than other components affecting calcium dynamics, so the pseudo-steady approximation can be applied. In addition to endogenous buffers (mainly proteins with calcium binding sites) that are always present in a cell, there is another reason that makes the study of the buffer effect on calcium dynamics very important. In experimental studies, calcium dynamics is visualized by loading a cell with a fluorescent indicator that acts as a high affinity mobile buffer. It is therefore crucial to know to what extent the exogenous buffer (a fluorescent indicator) can distort the original pattern.

We chose bistable systems for our study (Fig. 2a in Section 3 shows the typical behavior of the function $f(c)$ in Eq. (1.1) for one-variable systems) because they are known to maintain stable self-propagating waves [14]. Moreover, bistability is thought to be essential in the phenomenon of fertilization calcium waves [15]. The issues of existence and speed of traveling waves in bistable models in the presence of rapid mobile buffers were considered in a recent paper [16] (see also [14]). The authors of [16] proceeded with the calcium transport equation derived in [5]. Using a clever nonlinear transformation, they found the condition for the existence of traveling waves with the domination of high steady state concentration in the presence of a rapid buffer. However, as we show in this paper, their hypothesis, that the low buffer affinity limit yields a universal equation describing the buffer effect on the wave speed, does not hold. Our results indicate that the effect of calcium buffering on traveling waves in bistable systems can be drastically different depending on buffer affinity and system excitability. The latter is characterized by how close the unstable steady state concentration is to that of the lower stable steady state: the closer they are, the more excitable is the system. In particular, there is a threshold in system excitability above which traveling waves cannot be eliminated by a mobile buffer no matter how aggressive its characteristics are.

We now outline the structure of this paper. In Section 2 we describe our algorithm. We use a simple example of two-dimensional diffusion of a calcium spike in the presence of a mobile buffer to illustrate the convergence of the method and the applicability of the pseudo-steady approximation. In Section 3 we apply our algorithm to study the effect of a rapid mobile buffer on traveling waves in the simple one-variable models [16, 17]. Although these models are oversimplified compared to the physiologically relevant mechanisms, they are exactly solvable in the absence of buffers and there are also some asymptotic results in the case of rapid buffers. Thus, we can validate our numerical results and verify some

other theoretical predictions. In Section 4 we consider a more realistic two-variable model that becomes bistable for some parameter sets. Most of the qualitative conclusions drawn in the previous section appear to hold in this case as well. We also found a new feature: for certain parameter sets in the low excitability regime, the system undergoes bifurcation with the total buffer concentration as a bifurcation parameter. Thus, for some total buffer concentrations, there exist two stable traveling waves with very different velocities. As a consequence, in this case the system may sometimes exhibit a discontinuous "phase" transition from stable fast to stable slow waves as the total buffer concentration increases. This transition precedes the threshold beyond which no traveling wave with dominating high steady state concentration exists. Finally, in Section 5 we present the results of three-dimensional simulations of fertilization calcium waves. They illustrate the possible effect of a fluorescent indicator. The simulations have been run on realistic geometry with the realistic set of parameters and initial conditions. The results indicate strong interaction of buffers with initiating calcium spikes. The mobile buffers cause a delay in wave formation and, at a sufficient concentration, can prevent a wave.

2. NUMERICAL ALGORITHM

In this section, we document our algorithm designed for the reaction-diffusion systems containing a subsystem of fast reactions where characteristic times differ by two or more orders of magnitude. The idea of our algorithm is to combine time splitting [6], which is necessary for the separation of fast and slow reactions, with the pseudo-steady approximation applied to the fast subsystem. In many applications (see discussion in the previous section) the pseudo-steady approximation is well suited for obtaining a good quantitative solution by assuming the fast reactions are in equilibrium at all time after the initial rapid transient.

Let u_i, $i = 1, \ldots, n$, be the concentrations of various species involved in the dynamics and governed by a system of reaction-diffusion equations,

$$\frac{\partial u_i}{\partial t} = D_i \nabla^2 u_i + R_i, \qquad i = 1, \ldots, n, \tag{2.1}$$

with initial conditions

$$u_i(\boldsymbol{x}, 0) = u_i^0(\boldsymbol{x}), \tag{2.2}$$

and different boundary conditions for different cases that we study. Here D_i is the diffusion coefficient of the ith species. The effect of all the reactions on the ith species is represented by the source term R_i, which is a function of $u_1, \ldots, u_n$.

Assume that there are m different reactions with rates ν_j, $j = 1, \ldots, m$, taking place among the various species. Usually each ν_j is a nonlinear function of the concentrations of the species participating in this jth reaction. Thus with α_{ij} being the integer-valued stoichiometry matrix [8], which represents how many molecules of the ith species are produced (the positive sign) or consumed (the negative sign) due to the jth reaction, we have

$$R_i = \sum_{j=1}^{m} \alpha_{ij} \nu_j. \tag{2.3}$$

Without loss of generality, let the first k reactions be fast with rates $\nu_1, \ldots, \nu_k$, $k \le m$, respectively, while the remaining $m-k$ reactions are slow with rates $\nu_{k+1}, \ldots, \nu_m$, respectively. Diffusion is assumed to be a slow process which is usually the case in the length scale of interest.

In our algorithm, a typical time-step, say from T to $T+\Delta t$, is advanced in two stages. In both stages, the equations are coupled due to the reaction rate ν_j, $j = 1, \ldots, m$.

Stage I, due to fast reactions. We solve

$$\frac{\partial u_i}{\partial t} = \sum_{j=1}^{k} \alpha_{ij} \nu_j, \qquad i = 1, \ldots, n, \tag{2.4}$$

with given initial condition $u_i(\mathbf{x}, T)$, $i = 1, \ldots, n$, $\mathbf{x} \subset \mathbf{R}^3$. Its actual implementation involves the pseudo-steady approximation and will be discussed below. We let their solution be $\tilde{u}_i(\mathbf{x})$, $i = 1, \ldots, n$, after a time of Δt.

Stage II, due to slow reactions and diffusion. We solve

$$\frac{\partial u_i}{\partial t} = D_i \nabla^2 u_i + \sum_{j=k+1}^{m} \alpha_{ij} \nu_j, \qquad i = 1, \ldots, n, \tag{2.5}$$

with the same boundary conditions as for the governing equations and initial conditions $\tilde{u}_i(\mathbf{x})$ from the results in Stage I. The result that we obtain after a time of Δt is our numerical approximation to $u_i(\mathbf{x}, T+\Delta t)$.

We then repeat Stages I and II to compute the solution at successive times.

We now describe the implementation of Stage I in the algorithm. In Eqs. (2.4), it involves the $n \times k$ stoichiometry matrix $\alpha^{(f)} \equiv \alpha_{ij}$, $1 \le i \le n$, and $1 \le j \le k$. Assume the rank of the matrix $\alpha^{(f)}$ to be r; therefore $r \le \min(n, k)$. Its left null space $\mathcal{N}((\alpha^{(f)})^T)$ has a dimension of $n-r$, with a basis $\{\mathbf{l}_1, \ldots, \mathbf{l}_{n-r}\} \subset \mathbf{R}^n$. Using (2.4), it is then easy to verify that $\frac{\partial}{\partial t}(\mathbf{l}_i \cdot \mathbf{u}) = 0$, where $\mathbf{u} = (u_1, \ldots, u_n)^T$. Hence for fixed $\mathbf{x}$,

$$\sum_{j=1}^{n} \beta_{ij} u_j = I_i, \qquad i = 1, \ldots, n-r, \tag{2.6}$$

where β_{ij} is the jth component of the vector $\mathbf{l}_i$, and I_i is constant during this time step (but depending on $\mathbf{x}$), which should be updated from the initial conditions in Stage I. Equations (2.6) represent all the conservation relationships among the species with respect to fast reactions.

Let A be a non-singular $n \times n$ matrix such that its last $n-r$ columns are composed of $\{\mathbf{l}_1, \ldots, \mathbf{l}_{n-r}\}$. (For example, its first r columns can be composed of a basis $\{\mathbf{a}_1, \ldots, \mathbf{a}_r\} \subset \mathbf{R}^n$ for the column space of $\alpha^{(f)}$. Such a basis can be computed. However, we will employ a different choice below.) Therefore, Eqs. (2.4) are equivalent to

$$\sum_{i=1}^{n} A_{ip} \frac{\partial u_i}{\partial t} = \sum_{i=1}^{n} \sum_{j=1}^{k} A_{ip} \alpha_{ij} \nu_j, \qquad p = 1, \ldots, n, \tag{2.7}$$

since we can get Eqs. (2.4) from (2.7) and vice versa. The last $n-r$ equations correspond to Eqs. (2.6). We now apply the pseudo-steady approximation to the first r equations assuming

the fast reactions to be in rapid equilibrium; thus we will ignore the time derivative on the left hand side. Hence the first r equations can be approximated by

$$\sum_{j=1}^{k} \tilde{\alpha}_{pj} \nu_j = 0, \qquad p = 1, \ldots, r, \tag{2.8}$$

where $\tilde{\alpha}_{pj} \equiv \sum_{i=1}^{n} A_{ip} \alpha_{ij}$. In summary, in Stage I we solve Eqs. (2.6) and (2.8) to update u_i, $i = 1, \ldots, n$.

Our choice of matrix A makes it trivial to determine $\tilde{\alpha}_{pj}$: we just have to pick r rows of matrix $\alpha^{(f)}$ that correspond to "independent" variables. It also simplifies programming and makes the overall algorithm more efficient. The construction of the matrix A that we use is described below. Of course, such a choice is for convenience only and does not alter the final solutions. In fact, it can be rigorously proved that the solution to Eqs. (2.6) and (2.8) is independent of the choice of the matrix A, so long as its last $n - r$ columns are composed of $\{\mathbf{l}_1, \ldots, \mathbf{l}_{n-r}\}$ and it is non-singular (see Appendix A).

Since the rank of the matrix β in the linear equations (2.6) is always $n - r$, we can find r free variables among all the u_i so that the remaining $n - r$ of them can be expressed as a linear combination of such free variables by performing Gaussian elimination. The free variables can be read off from the structure of the echelon matrix U resulting from the Gaussian elimination. Putting such relations back into Eqs. (2.8), we obtain a system of r nonlinear algebraic equations for the r independent u_i. We solve this nonlinear system using the Newton's method, with a good initial guess being the initial conditions for such u_i in Stage I.

We now describe how we construct the matrix A. Let the location of the free variables be $i = i_1, i_2, \ldots, i_r$. For each i_j, $j = 1, \ldots, r$, we construct a unit vector in $\mathbf{R}^n$ whose components are zero except at the i_j position where we assign a value of 1. For example, if $i_1 = 2$, then we construct the vector $(0, 1, 0, \ldots, 0)^T$. It is easy to see that this set of r vectors, $\{\mathbf{b}_1^T, \ldots, \mathbf{b}_r^T\}$, and the $n - r$ rows of the matrix U form n linearly independent vectors, since together they form a $n \times n$ upper triangular matrix with non-zero diagonal entries. But the row space of U is the same as the row space of the matrix β, which is also equal to the left null space of $\mathcal{N}((\alpha^{(f)})^T)$; therefore $\{\mathbf{b}_1, \ldots, \mathbf{b}_r\}$ and $\{\mathbf{l}_1, \ldots, \mathbf{l}_{n-r}\}$ are linearly independent. Hence $\{\mathbf{b}_1, \ldots, \mathbf{b}_r\}$ can be employed in the first r columns in the construction of the matrix A, giving

$$A = (\mathbf{b}_1, \ldots, \mathbf{b}_r, \mathbf{l}_1, \ldots, \mathbf{l}_{n-r}). \tag{2.9}$$

Correspondingly, the matrix $\tilde{\alpha}$ reduces to a choice of the (i_j)th, $j = 1, \ldots, r$, rows of the matrix $\alpha^{(f)}$.

In the implementation of Stage II, any standard algorithm can be employed. Currently we use a finite volume method [18] for the implicit time discretization of the diffusion term, and an explicit treatment of the nonlinear reactions in Eqs. (2.5). This gives us numerical stability and avoids the solving of nonlinear equations in this step. By itself, the local discretization error in this step is first order in time and second order in space.

There are two additional sources of error for this time splitting method. First, we have broken down the original governing equations in a typical time step Δt into two simpler steps (Stages I and II), each with simpler Eqs. (2.4) and (2.5), respectively. Even if we solve these simpler equations exactly, we already invoke the time splitting error. The second

source of error comes from the pseudo-steady approximation. As we discussed in Section 1, such approximation gets better when there is a substantial difference in characteristic times between fast and slow processes. In our actual numerical experiments, numerical stability and convergence are observed, with an overall accuracy of first order in time.

This algorithm has been implemented as a part of the Virtual Cell software. Its development has been motivated by the requirement to fully automate the treatment of fast reaction kinetics within the Virtual Cell modeling environment. To run a simulation with the Virtual Cell, a physiological model (reactions, diffusion, and membrane fluxes topologically organized by cell compartments), a geometric model, which represents anatomical features, membrane locations, and the domain size, and a set of simulation specific requirements (initial conditions, boundary conditions, external stimulus, and the selection of "fast" reactions) have to be specified (http://www.nrcam.uchc.edu/). From this specification, a mathematical model is automatically constructed including simplifications based on mass conservation relationships and, if necessary, the pseudo-steady approximation discussed in this paper. A major feature of the Virtual Cell design is that the description of the physiology is decoupled from the choice of an appropriate mathematical treatment for a given simulation, which depends (among other things) on the spatial and time scales of the physiological questions being asked.

The biochemical reactions, anatomical features, geometry, and simulation specification are graphically edited within the Virtual Cell Java applet [19] running within a web browser. All that a user has to do to invoke the "fast" algorithm is specify in the reaction editor the reactions that are considered fast. The time splitting, stoichiometry analysis, and pseudo-steady approximation are then automatically performed and, for spatial problems, the resulting system of partial differential and algebraic equations is sent to our solver environment on a remote server, where code is generated and linked into existing C++ numerical libraries. In the case of a non-spatial (compartmental) problem, the system of ordinary differential and algebraic equations is solved within the web browser and is accompanied by a local sensitivity analysis. In either case, the results are then displayed within the applet.

We now illustrate how our method works with a simple example of two-dimensional diffusion of a calcium spike in the presence of a mobile buffer, a situation when calcium is spontaneously released from a channel (a calcium "spark" [20]) or injected at a specific location in the cytoplasm loaded with a fluorescent dye. The system is described by Eqs. (1.3) with $f \equiv 0$. Thus in this simple case, we have two variables $u_1 = c$ and $u_2 = b$ coupled by one fast reaction. Using our approach, we perform time splitting and pseudo-steady approximation that result in a "slow" subsystem,

$$\begin{aligned} \frac{\partial c}{\partial t} &= D_c \nabla^2 c, \\ \frac{\partial b}{\partial t} &= D_b \nabla^2 b, \end{aligned} \tag{2.10}$$

and a "fast" subsystem consisting of a "fast" invariant (see (2.6)),

$$c + b = I, \tag{2.11}$$

and a nonlinear algebraic equation,

$$c(b_t - b) = Kb, \tag{2.12}$$

where $K \equiv k_{off}/k_{on}$ is the dissociation constant. The fast and slow subsystems are then solved in two steps as described above.

To test the validity of our algorithm, we will compare its numerical results with those from a regular algorithm which does not perform time splitting and uses a small time step all the time to resolve the fast reaction (this type of algorithm is employed in Stage II of our approach). Both methods are used to run simulations on a two-dimensional square domain with dimension $(-L, L) \times (-L, L)$ with initial conditions

$$c(\mathbf{x}, 0) = c_0 + \frac{c_1}{\sigma\sqrt{2\pi}} \exp\left(-\frac{|\mathbf{x}|^2}{2\sigma^2}\right), \qquad b(\mathbf{x}, 0) = \frac{b_t c(\mathbf{x}, 0)}{K + c(\mathbf{x}, 0)}, \tag{2.13}$$

and zero flux boundary conditions for both species.

In this example, we use the system of units which is often convenient in physiological applications. In this system, length is measured in microns (μm), time in milliseconds (ms), and concentration in micro molars (μM, 1 M = 1 mole/litre). In these units, the parameter set employed in the simulations is as follows: $L = 10$, $D_c = 5 \times 10^{-3}$, $D_b = 5 \times 10^{-2}$, $K = 0.24$, $\sigma = 0.5$, $c_0 = 0.05$, $c_1 = 10.0$, and $b_t = 10.0$. We will use different values for k_{on} thus varying the characteristic time of the fast reaction.

We first demonstrate the convergence of the regular algorithm. For that matter, we run simulations for the relatively large $k_{on} = 0.25$ (the numerical convergence for smaller k_{on} is easier to achieve), with the decreasing time step Δt and mesh size Δx such that $\Delta t \propto (\Delta x)^2$. A spatial mesh size of $\Delta x_i = h/2^i$, $i = 0, 1, 2$, and the corresponding time step Δt_i are used to determine the solution $U_i(\mathbf{x})$ of either c or b at some time T. Since we expect the error to be $O(\Delta t) + O((\Delta x)^2)$, it can be shown that the ratio

$$r \equiv \frac{\|U_0 - U_1\|_2}{\|U_1 - U_2\|_2} \tag{2.14}$$

should be close to 4 when h is small. In Table I we present the results for this ratio obtained with $h = 0.5$ and $\Delta t_0 = 0.01$, $\Delta t_1 = 0.0025$, and $\Delta t_2 = 0.000625$. The good agreement with the predicted value confirms the expected convergence of the general algorithm.

From now on, we regard the numerical solutions computed in this way using $\Delta x = 0.5$ and $\Delta t = 0.01$ as the standard solutions (we estimate that for $T \geq 5$, they are accurate within 0.7%). To study the effect of time splitting and pseudo-steady approximation, we then compare these solutions for various k_{on} to the one obtained using our fast algorithm for the same discretization parameters. Note that when using the pseudo-steady approximation, we need only K and do not require a value for k_{on}. In this example, the characteristic time of the fast reaction can be estimated as $\tau_{fast} = 1/(k_{on} b_t)$ while time scales of slow diffusion are $\tau_c = \sigma^2/D_c$ and $\tau_b = \sigma^2/D_b$ for calcium and the buffer, respectively.

TABLE I
Ratio r of Eq. (2.14) for the Variables c and b at Varying Time

Time, T (ms)	Variable c	Variable b
10	4.54539	4.41447
20	4.23496	4.20957
30	4.15328	4.14222
40	4.11376	4.10754

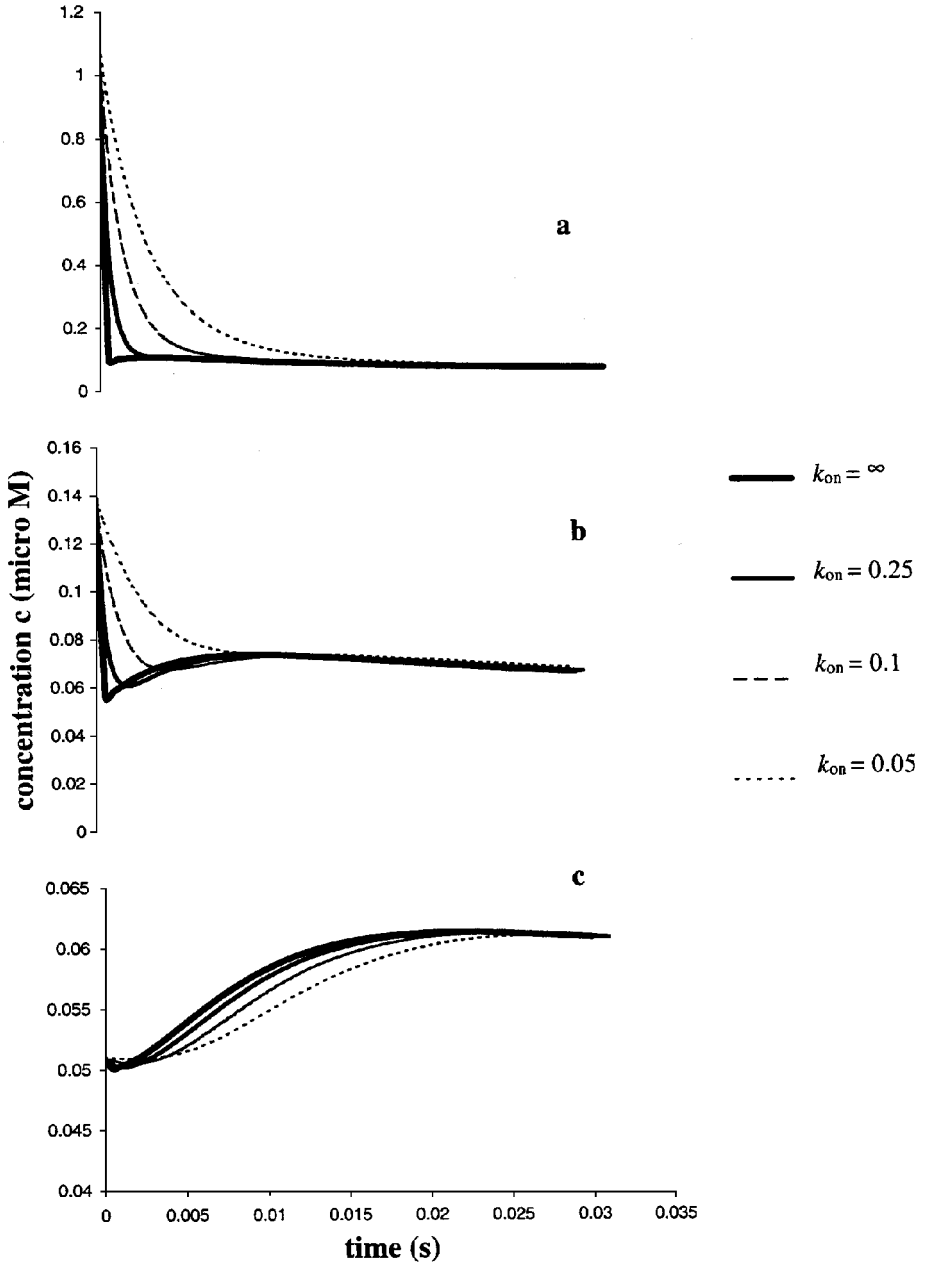

FIG. 1. Results of the "full" solution for $c(\mathbf{x}, t)$ obtained with increasing reaction rates k_{on}, as compared to those of the "fast" algorithm (solid lines). (a) $\mathbf{x} = (1, 0)$; (b) $\mathbf{x} = (1.5, 0)$; (c) $\mathbf{x} = (1.5, 1.5)$.

As discussed in Section 1, the pseudo-steady approximation should give accurate results if $\tau_{fast} \ll \min(\tau_c, \tau_b)$, which leads to $k_{on} \gg \max(D_c, D_b)/(b_t \sigma^2) = 0.02$. In Fig. 1 we present the time history of $c(\mathbf{x}, t)$ for some $\mathbf{x}$. We see that as k_{on} increases, the standard solutions (computed using the same Δx and Δt) approach the pseudo-steady approximation solution. In fact, when $k_{on} \geq 0.25$, the two profiles virtually coincide. Such results show that pseudo-steady approximation is an accurate algorithm when k_{on} is large. Moreover, it is efficient because the fast time scale has been filtered off.

In the following sections we use our algorithm to study the effect of a mobile buffer on calcium waves assuming calcium buffering is fast enough for the pseudo-steady approximation be applicable.

3. BUFFERED TRAVELING WAVES IN ONE-VARIABLE BISTABLE MODELS

We start our application with very simple one-variable bistable models described by Eq. (1.1) where f is a function of one variable, $f(c)$, that typically behaves as shown in Fig. 2a. It is important for bistability that $f(c)$ has three zeros $C_{\min} < C_0 < C_{\max}$, which in the absence of diffusion would correspond to the concentration values in two stable steady states separated by an unstable steady state. In physiological applications the system usually rests at a steady state with lower concentration $C_{\min}$. Thus, to excite the system, we have to overcome the concentration barrier $C_0 - C_{\min}$. Therefore, the position of the unstable steady state concentration C_0 with respect to $C_{\min}$ and $C_{\max}$ characterizes the system excitability. In the presence of diffusion, bistable models are known to allow for the solutions of a traveling wave type $c(x + vt) = c(\xi)$ with a constant wave speed v [14, 21] (a wave with positive wave speed v travels to the left).

We consider two models: one employs a piecewise linear function f (a PL model), and the other uses a cubic polynomial (a CP model) [14, 16, 17]. Both the high and low excitability regimes in each model are studied. In the absence of buffers, both models admit exact analytical solutions with explicit wave speeds. There are also some formal asymptotic results available for fast-buffered traveling waves in one-variable bistable models, which allow us to assess the accuracy of our numerics. Thus, we pursue two goals when applying our numerical approach to the oversimplified one-variable models. First, we validate, whenever

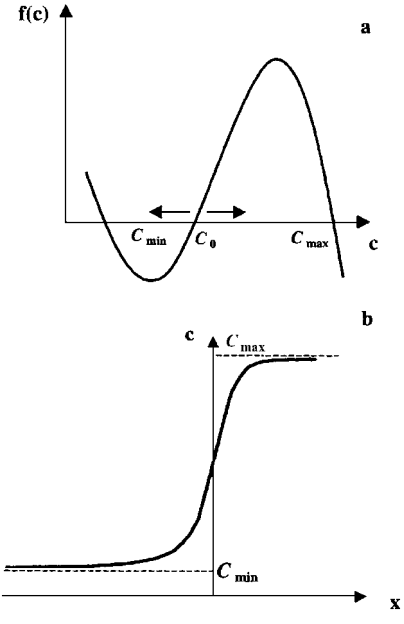

FIG. 2. (a) Typical shape of the function f in one-variable bistable models. (b) Typical traveling wave profile in one-variable models.

possible, our algorithm against exact analytical results, and second, we verify predictions based on our theoretical analysis.

3.1. Theoretical predictions. The function f in the PL model is described by the equation

$$f(c) = J_0\theta(c - C_0) - \Gamma(c - C_{\min}), \tag{3.1}$$

where θ is a step function with

$$\theta(x) = \begin{cases} 1 & \text{if } x \geq 0 \\ 0 & \text{if } x < 0. \end{cases}$$

The first term on the right hand side of Eq. (3.1) is the rate of calcium release from the internal stores through calcium channels [17]. Here, J_0 denotes the amplitude of this rate and C_0 is the threshold calcium concentration above which the channels get activated. The second term on the right hand side of Eq. (3.1) describes the rate of calcium uptake back into internal stores due to calcium pumps. This rate is assumed to be linear with respect to current calcium concentration in the PL model. Obviously, in this model $C_{\max} = J_0/\Gamma + C_{\min}$. The traveling wave speed in the PL model is

$$v_0 = \sqrt{\frac{J_0 D_c}{C_0 - C_{\min}}}\frac{1 - 2\rho}{\sqrt{1-\rho}}, \qquad \text{where } \rho = \frac{\Gamma}{J_0}(C_0 - C_{\min}). \tag{3.2}$$

In the CP model

$$f(c) = \frac{J_0}{C_{\max}^3}(c - C_{\min})(c - C_0)(C_{\max} - c), \tag{3.3}$$

and the wave speed is

$$v_0 = \sqrt{\frac{J_0 D_c}{2C_{\max}}}\frac{C_{\max} - 2C_0 + C_{\min}}{C_{\max}}. \tag{3.4}$$

In the presence of a mobile buffer, the system is governed by Eqs. (1.3). One can prove that this system also has a unique monotone traveling wave solution connecting two stable steady states and a unique wave speed [22, Theorem 2.1, p. 15]. In the limit of fast buffering, one can derive an asymptotic wave speed (see Appendix B)

$$v = \left(\int_{C_{\min}}^{C_{\max}} f(c)\left(1 + \frac{D_b b_t K}{D_c(K+c)^2}\right)dc\right) \times \left(\int_{-\infty}^{\infty}\left(1 + \frac{b_t K}{(K+c)^2}\right)\left(1 + \frac{D_b b_t K}{D_c(K+c)^2}\right)\left(\frac{dc}{d\xi}\right)^2 d\xi\right)^{-1}. \tag{3.5}$$

In the limit of low buffer affinity $K/C_{\max} \gg 1$, as shown in Appendix B, this equation reduces to a well known expression for the wave speed [16, 17],

$$v = v_0\left(1 + \frac{D_b b_t}{D_c K}\right)^{1/2}\left(1 + \frac{b_t}{K}\right)^{-1}, \tag{3.6}$$

where v_0 is the speed of a wave in the absence of buffering. In addition to direct wave speed measurements described in the next subsection, Eq. (3.5) provides an alternate way of determining the wave speed from simulation results.

Although Eq. (3.5) is not explicit, we can get some important insights by analyzing it. Define $\gamma \equiv D_b b_t / D_c$. Let us fix $C_{\min}$ and $C_{\max}$ and vary the system excitability by changing C_0. To emphasize this fact, we write $f(c) \equiv f(c, C_0)$. Then from Eq. (3.5), the sign of the wave speed (and, consequently, the condition for the existence of the traveling wave with the domination of the higher steady state concentration) is determined by the sign of the integral

$$V \equiv \int_{C_{\min}}^{C_{\max}} f(c, C_0) \left(1 + \frac{\gamma K}{(K + c)^2}\right) dc, \tag{3.7}$$

which depends both on system excitability and buffer characteristics. This is in agreement with the result of [16] obtained by means of a particular nonlinear transformation. We further define

$$G(C_0) \equiv \int_{C_{\min}}^{C_{\max}} f(c, C_0)\, dc, \qquad H(C_0, K) \equiv \int_{C_{\min}}^{C_{\max}} \frac{f(c, C_0)}{(K + c)^2}\, dc.$$

Since it is easy to check for the PL and CP models that $\partial f / \partial C_0 < 0$, hence $\partial G / \partial C_0 < 0$ and $\partial H / \partial C_0 < 0$. Then there are unique values of C_0, $\bar{c}$, and $\tilde{c} = \tilde{c}(K)$, such that $G(\bar{c}) = 0$ and $H(\tilde{c}, K) = 0$. Since $H(\bar{c}, K) < 0$, then $\tilde{c} \in (C_{\min}, \bar{c})$ and $\tilde{c}$ tends to $\bar{c}$ as K increases.

We now fix K and consider any $C_0 \in (C_{\min}, \tilde{c}]$ (high excitability regime); then the integral (3.7) is positive irrespective of the value of γ. In other words, the traveling wave speed is always positive no matter what total buffer concentration we introduce and how large its diffusion coefficient is, as long as the system excitability is sufficiently high. On the other hand, when $C_0 \in (\tilde{c}, \bar{c})$ (the low excitability regime), there is a threshold value of γ,

$$\gamma_{C_0} \equiv -\frac{1}{K} \frac{G(C_0)}{H(C_0, K)}, \tag{3.8}$$

such that for $\gamma > \gamma_{C_0}$, there are no traveling waves with positive speeds. If $C_0 \geq \bar{c}$, wave speed is negative (the lower steady state concentration dominates) for any combination of buffer parameters.

Finally, it is interesting to note that the dependence of the numerator in Eq. (3.5), V, on D_b is drastically different in regions of the high and low excitability: for $C_0 < \tilde{c}$ the wave speed V is positive and $\partial V / \partial D_b > 0$, while for $C_0 \in (\tilde{c}, \bar{c})$, $\partial V / \partial D_b < 0$. Thus, in situations when the numerator of Eq. (3.5) plays a dominant role in determining the wave speed, an increase of the buffer diffusion coefficient may speed up or reduce the wave velocity in the high and low excitability modes, respectively. In the low affinity limit $K / C_{\max} \to \infty$, when the low excitability region is disappearing because $\tilde{c} \to \bar{c}$, we expect the wave speed to be an increasing function of D_b for any $C_0 \in (C_{\min}, \bar{c})$, in accordance with Eq. (3.6). However, in the case of a high affinity buffer and low system excitability ($C_0 \in (\tilde{c}, \bar{c})$), this dependence might be the reverse. In this case, the growth of D_b will lead to a point $\gamma = \gamma_{C_0}$ at which the traveling wave with a positive wave speed ceases to exist. Our numerical results presented below confirm such a conclusion.

3.2. Numerical results. We first describe our choice of the parameter values employed in the PL and CP models. The calcium diffusion coefficient in the cytoplasm, D_c, is thought to be 3–4 times smaller than in water and estimated as 220 μm^2/s [23]. But because of the endogenous buffers that are always present in a cell, the effective calcium diffusion can be 10–50 times slower. Since the endogenous buffers compete for calcium with exogenous (added) buffers, one should explicitly introduce both types of buffers in the simulation. We use this approach in our three-dimensional (3D) simulations of fertilization calcium waves (see Section 5). In this section, however, it is beneficial to keep models simple in order to facilitate comparison with the exact results. Therefore, in our one-dimensional (1D) simulations we assume the reduced effective calcium diffusion coefficient $D_c = 22$ μm^2/s to account for the effect of endogenous buffers and explicitly introduce only one mobile exogenous buffer into a system. In the physiological range, the maximal calcium concentration is of the order of 1–2 μM and the wave speed is in the range of 1–20 μm/s.

The parameter values that we use in simulations satisfy these constraints. In the PL model we use $C_{\min} = 0.05$ μM, $J_0 = 1.5$ μM/s, and $\Gamma = 1.0$ s^{-1}, which yield $C_{\max} = 1.55$ μM. As we mentioned above, we will consider two different levels of system excitability, relatively high excitability at $C_0 = 0.15$ μM and relatively low excitability at $C_0 = 0.55$ μM. It follows then from Eq. (3.2) that

$$v_{0,\text{exact}} = \begin{cases} 16.2964\ \mu\text{m/s} & \text{at } C_0 = 0.15\ \mu\text{M (high excitability)} \\ 3.3166\ \mu\text{m/s} & \text{at } C_0 = 0.55\ \mu\text{M (low excitability).} \end{cases} \tag{3.9}$$

In the CP model we use $C_{\min} = 0$, $C_{\max} = 1.0$ μM, $J_0 = 20$ μM/s and assign the values of 0.1 and 0.4 μM to C_0 for the high and low excitability, respectively. For this set of parameters Eq. (3.4) yields

$$v_{0,\text{exact}} = \begin{cases} 11.8659\ \mu\text{m/s} & \text{at } C_0 = 0.1\ \mu\text{M (high excitability)} \\ 2.9665\ \mu\text{m/s} & \text{at } C_0 = 0.4\ \mu\text{M (low excitability).} \end{cases} \tag{3.10}$$

In most simulations, we use a step function as initial calcium distribution,

$$c(x, 0) = \begin{cases} C_{\max}, x \le 0 \\ C_{\min}, x > 0, \end{cases}$$

and a buffer being initially in equilibrium with calcium; in some PL model simulations, however, we initiated the wave by a calcium spike of a Gaussian form. In these numerical experiments, by the time the concentration behind the wave front approaches its steady state value, the wave has practically settled in its traveling wave profile.

To measure the speed of a simulated traveling wave after the transient dies down, we evaluate the average velocity of the point with the same prescribed concentration over a certain time. The coordinate of the point at the end of the time period is determined by means of interpolation. The interpolation error introduced in the wave speed measurement can be suppressed by taking the average over several measurements. In our practical implementation we repeated measurements by varying time and locations on the wave front until the standard error becomes less than 1%. The measured speed should be time independent, and the same for any prescribed concentration that we pick. These requirements serve as a check whether the wave has settled down or not. In order to compare with the exact wave speed, we have to take a sufficiently large computational domain to ensure that the boundaries of

the computational domain, where we impose zero flux boundary conditions, do not affect the traveling wave. In some cases this requirement leads to a rather large computational domain.

Taking all the precautions described above, we first perform experiments for cases without buffers. A trade off between accuracy and reasonable time of computation was achieved at the mesh size $\Delta x = 0.2$ μm and the time step $\Delta t = 1$ ms with up to 5000 mesh points in the domain and the simulated time in the range of 15–200 s. The numerical results obtained with these discretization parameters are as follows. For the PL model,

$$v_{0,\mathrm{num}} = \begin{cases} 16.1763\ \mu\mathrm{m/s} & \text{at } C_0 = 0.15\ \mu\mathrm{M} \text{ (high excitability)} \\ 3.2859\ \mu\mathrm{m/s} & \text{at } C_0 = 0.55\ \mu\mathrm{M} \text{ (low excitability),} \end{cases} \tag{3.11}$$

and for the CP model,

$$v_{0,\mathrm{num}} = \begin{cases} 11.8292\ \mu\mathrm{m/s} & \text{at } C_0 = 0.1\ \mu\mathrm{M} \text{ (high excitability)} \\ 2.9641\ \mu\mathrm{m/s} & \text{at } C_0 = 0.4\ \mu\mathrm{M} \text{ (low excitability).} \end{cases} \tag{3.12}$$

Comparing such wave speeds with the exact values in (3.9) and (3.10), we conclude that the numerical results are accurate within 1%. It is also not surprising to find that the PL model simulation is not as accurate because the function (3.1) employed in this model is not continuous.

We use similar discretization parameters to simulate systems in the presence of buffers. In this case we check our numerical results against (i) the asymptotic solution (3.6) in the low affinity limit, (ii) the critical value (3.8) at which the wave speed becomes zero, and (iii) we use the wave speed (3.5) to double check results in the general circumstances. All the tests indicate that the numerical results we present below are accurate to within 2% of the theoretical values.

We first consider the high excitability mode and vary buffer affinity at a fixed buffer diffusion coefficient $D_b = 10$ μm^2/s. The plots of the normalized speed v/v_0 vs the binding ratio b_t/K are shown in Fig. 3. Both the PL and CP models exhibit qualitatively similar behavior. The solid lines represent the exact dependencies (3.6) in the low affinity limit $K/C_{\max} = \infty$. As expected, the numerical points at $K = 100$ μM follow closely the theoretical curve of the low affinity limit. (Recall that $C_{\max}$ are 1.55 μM and 1 μM in the PL and CP model, respectively.) Somewhat surprisingly, the low affinity limit also provides a good approximation for $K = 1$ μM. However, the results in the high affinity case, $K = 0.1$ μM, deviate significantly from Eq. (3.6). Thus, the hypothesis made in [16, p. 118], that when K is small the speed of the traveling wave can still be approximated by Eq. (3.6), does not hold even in the case of high excitability (Eq. (3.5), however, holds). In the case of low excitability, such a claim produces an even more erroneous result, because the wave speed from (3.6) is always positive. In reality, as we have seen in Subsection 3.1 and demonstrated by numerics later on, at some parameter sets the wave speed can become negative.

Next, we keep the buffer affinity high ($K = 0.1$ μM) and vary the excitability. In the low excitability regime in both models there is a threshold buffer concentration $b_{t,c}$ above which there exists no traveling wave with the dominating high steady state concentration. The theoretically predicted values (see Eq. (3.8)) for the sets of parameters employed, $b_{t,c} = 18.29$ μM for the PL model and $b_{t,c} = 0.7154$ μM for the CP model, are in excellent agreement with the numerical results (see Figs. 4a and 4b). It is clear from both figures that if we continuously increase system excitability, there will be a threshold above which the

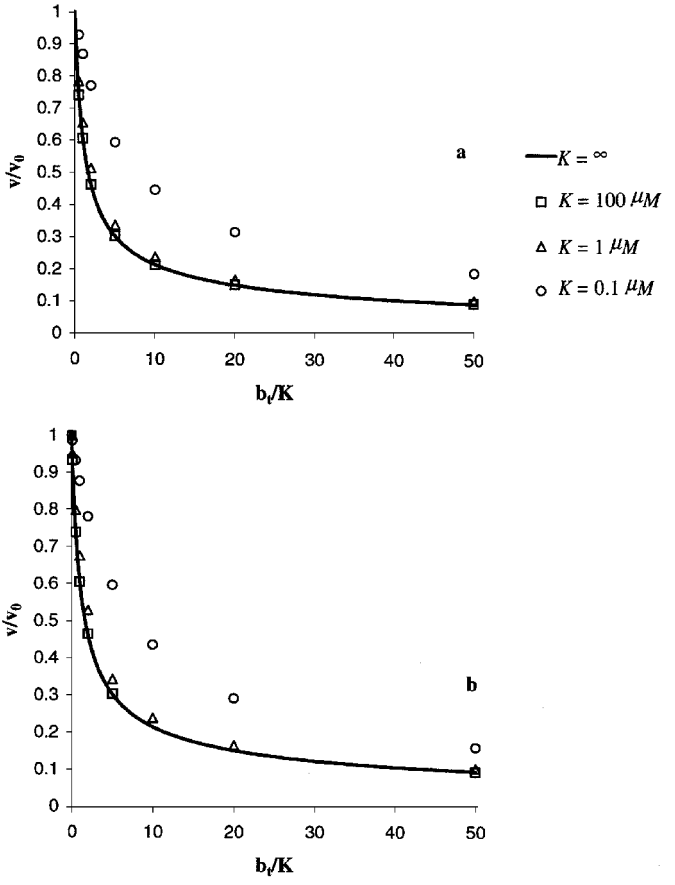

FIG. 3. Normalized wave speed vs buffer binding ratio for varying buffer affinity in the high excitability mode for $D_b = 10\,\mu\text{m}^2/\text{s}$. (a) PL model; (b) CP model.

wave with the dominating high concentration exists no matter how aggressive the buffer characteristics are. This conclusion is also consistent with the theoretical predictions.

It is interesting to note that the solution $c(\xi)$ for the zero wave velocity has a wave-like profile (see Fig. 2b). This means that a bistable system allows for a spatially non-uniform steady state with non-zero calcium fluxes, production, and consumption at the wave front (of course, this is also true in the absence of buffers). Physically, this is possible only if there are permanent sources of energy necessary for calcium pumping. Above the critical buffer concentration, a traveling wave with the dominating low steady state concentration exists. In other words, it moves in the opposite direction, or has a negative speed. It is interesting to see how the absolute value of speed will change if we further increase buffer concentration. Figure 5 shows that after the initial increase, it goes down. From the physiological point of view, the wave becomes self-extinguishing above the critical buffer concentration and cannot be initiated by a calcium spike over the uniform steady state with low calcium concentration $C_{\min}$.

Finally, we study the change in wave speed behavior with respect to the buffer diffusion coefficient at varying excitability. As one might expect from the theoretical analysis in Subsection 3.1, the results presented in Fig. 6 indicate that for a fixed buffer affinity, a larger

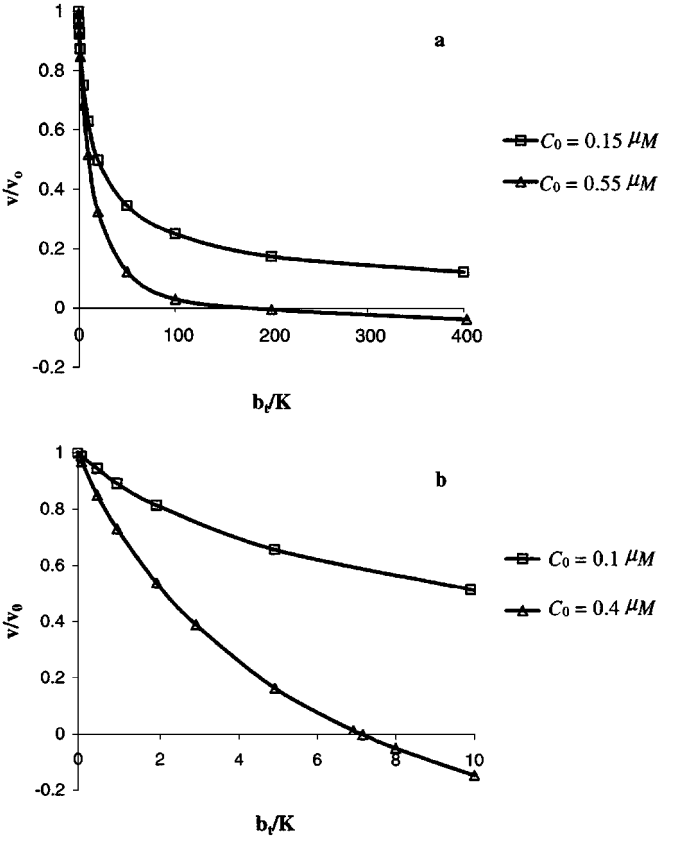

FIG. 4. Normalized wave speed vs buffer binding ratio for varying excitability in the case of a high affinity buffer, $K = 0.1\,\mu$M, for $D_b = 50\,\mu\text{m}^2/\text{s}$. (a) PL model; (b) CP model.

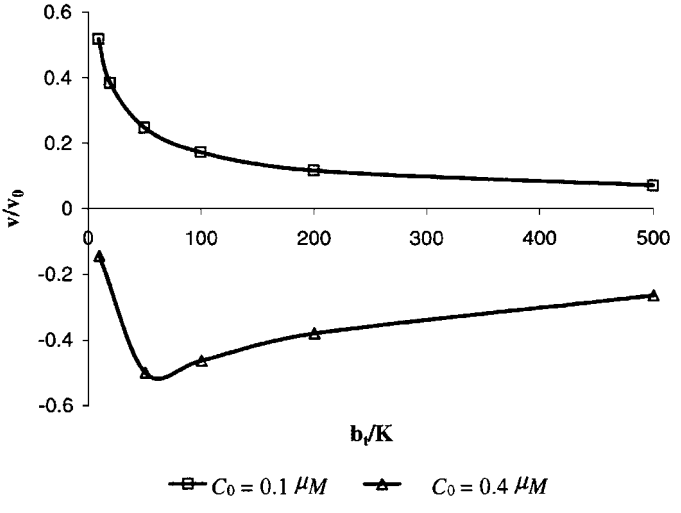

FIG. 5. Normalized wave speed vs buffer binding ratio for larger concentrations of a high affinity buffer in the CP model, $K = 0.1\,\mu$M, $D_b = 50\,\mu\text{m}^2/\text{s}$.

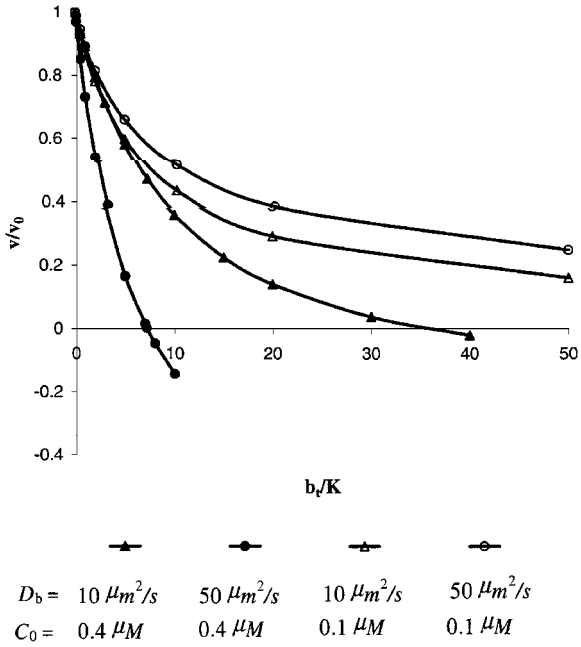

FIG. 6. Normalized wave speed vs buffer binding ratio for varying system excitability and buffer diffusion in the CP model at $K = 0.1\ \mu$M.

diffusion coefficient leads to a faster wave in the regime of high excitability, but the wave will be slower in the low excitability mode. In fact, with increasing D_b (at a fixed total buffer concentration), the wave slows down to zero speed at some critical value of D_b, when the wave ceases to exist physiologically.

Overall, as one would expect, adding a buffer slows down the wave speed in all numerical experiments. This is because calcium buffering leads to an effective decrease in both calcium release from channels and calcium diffusion [17].

4. BUFFERED TRAVELING WAVES IN A TWO-VARIABLE MODEL

In this section we study the effect of a rapid mobile buffer on traveling calcium waves in a more realistic two-variable model of calcium dynamics. This is a simplified Li–Rinzel model [24] which has been successfully applied in the studies of the calcium dynamics [3, 15, 25]. It is based on the detailed eight-state De Young–Keizer model of a ($InsP_3$)-sensitive calcium channel [26]. This channel consists of four subunits, each with binding sites for $InsP_3$ and Ca^{2+}. Calcium flux through the channel is regulated by $InsP_3$ and Ca^{2+} binding to these sites. In this paper we assume for simplicity that the $InsP_3$ concentration is constant so that it does not enter the governing equations. This simplification is appropriate in certain experimental conditions [11, 15], although the complete model should include the dynamics of $InsP_3$ [3, 4, 11]. According to the De Young–Keizer model, each of the four channel subunits has two Ca^{2+} binding sites; one activates the channel and the other inhibits it. It is further assumed that, for a channel to be open, three of the four subunits should have a bound activation site and a free inhibition site. The simplification made in [24] takes advantage of the fact that both the $InsP_3$ binding and the Ca^{2+} binding to the activation site

are much faster than the Ca^{2+} binding to the inhibition site. Thus, calcium binding to the inhibition site is the only slow process in the channel kinetics in the Li–Rinzel model.

In the absence of a mobile buffer, the model contains two variables: the calcium concentration, c, and the probability h that the inhibition site is free of calcium. These variables are governed by the equations

$$\begin{aligned} \frac{\partial c}{\partial t} &= D_c \nabla^2 c + f(c,h), \\ \frac{\partial h}{\partial t} &= g(c,h), \end{aligned} \tag{4.1}$$

where

$$f(c,h) = J_0 \left(\frac{ch}{c + d_{act}} \right)^3 - V_m \frac{c^2}{c^2 + K_p^2} + L \tag{4.2}$$

$$g(c,h) = k_{on} \left(d_{inh} - (d_{inh} + c)h \right). \tag{4.3}$$

The first term in (4.2) describes the rate of calcium release from a channel with an amplitude J_0 and a dissociation constant for the activation binding site d_{act}. The second term is the rate of calcium uptake through pumps with a maximal value V_m and a dissociation constant K_p for the calcium binding to a pump. The model also accounts for the constant leak of calcium, with rate L, from the internal stores to the cytoplasm. Equation (4.3) describes calcium binding to the inhibition sites, with a rate constant k_{on} and a dissociation constant d_{inh}.

For some parameter sets, the model is bistable [15]. Although the simple analysis of the previous section, which is valid for one-variable bistable models, does not apply in this case, it is likely that the relative location of steady state concentrations (for Eqs. (4.1) without diffusion) may still control the system excitability. Thus, we again consider two modes when the unstable steady state concentration C_0 is close to and far from the low steady state calcium concentration $C_{\min}$. In analogy with the previous section, we will call them the modes of high and low excitability, respectively. The corresponding sets of parameter values and the steady state concentrations are documented in Table II and the resulting nullclines with $f(c,h) = 0$ and $g(c,h) = 0$ are plotted in Fig. 7.

TABLE II
Parameter Sets Providing Bistability of the Li–Rinzel Model with High and Low Excitability

Parameter	Units	High excitability	Low excitability
J_0	μM s^{-1}	100	110
d_{act}	μM	0.7	0.7
V_m	μM s^{-1}	1.0	1.0
K_p	μM	0.25	0.1
L	μM s^{-1}	0.0151	0.1755
k_{on}	$(\mu\text{M})^{-1}$ s^{-1}	4.0	4.0
d_{inh}	μM	0.6	0.5
$C_{\min}$	μM	0.05	0.05
C_0	μM	0.1	0.3
$C_{\max}$	μM	1.187	1.022

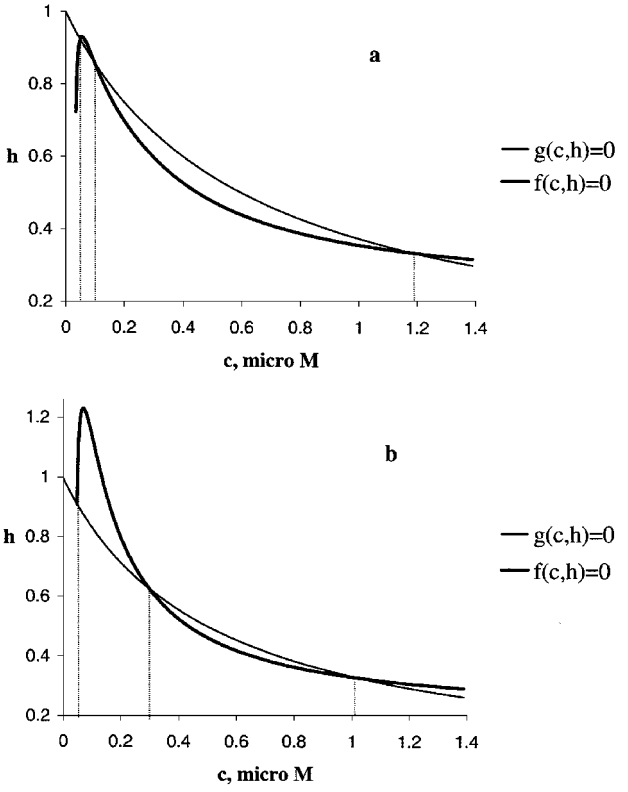

FIG. 7. Nullclines of the Li–Rinzel model for the cases of high (a) and low (b) excitability.

With a larger set of parameters being involved in the model, there are various ways of changing system excitability. In particular, one can vary the relative positions of the steady state calcium concentrations with little effect on the wave speed. This is in contrast to the one-variable models where a change from high to low excitability automatically leads to a decrease in the wave speed, as can be seen from Eqs. (3.2) and (3.4). As seen from Table II, we can now switch the system from high to low excitability by increasing the pump affinity and channel inhibition site affinity to calcium, while keeping the parameters J_0 and d_{act} (that control the wave speed [17]) essentially the same. (As a consequence, there is also a considerable change in the leak constant to maintain the flux balance at the low steady state with a fixed $C_{\min} = 0.05\,\mu$M.) As a result, we get similar wave speed values: $v_0 = 16.41\,\mu$m/s for the high excitability mode, and $v_0 = 15.80\,\mu$m/s for the low excitability mode, as opposed to the results (3.9), (3.10) obtained for the one-variable models. However, in the presence of a mobile buffer, the system with low excitability turns out to be "reluctant" in maintaining fast stable traveling waves. As the total buffer concentration increases, the system undergoes a discontinuous "phase" transition to the states with slow stable traveling waves (see Fig. 10 and discussion at the end of the section).

In the numerics above, we have used a step function for the initial calcium concentration, while the initial conditions for h are determined from $g(c(\mathbf{x}, 0), h) = 0$. Zero flux boundary conditions for c are imposed. As in the earlier sections, we observe numerical convergence upon decreasing mesh sizes and time steps. The accuracy is within 1% error when $\Delta t = 1$ ms and $\Delta x = 0.25\,\mu$m, with 4000–4500 points in the computational domain.

We use similar discretization parameters to simulate the system in the presence of a buffer. In this case the resulting set of equations becomes

$$\frac{\partial c}{\partial t} = D_c \nabla^2 c + f(c,h) + R \tag{4.4}$$

$$\frac{\partial h}{\partial t} = g(c,h), \tag{4.5}$$

$$\frac{\partial b}{\partial t} = D_b \nabla^2 b - R \tag{4.6}$$

with R from Eq. (1.3c). We again assume fast buffering. The wave speed (3.5), which now takes the form

$$v = \left(\int_{-\infty}^{\infty} \left(1 + \frac{D_b}{D_c} \frac{\partial b}{\partial c} \right) f(c(\xi), h(\xi)) \frac{dc}{d\xi} \, d\xi \right) \times \left(\int_{-\infty}^{\infty} \left(1 + \frac{\partial b}{\partial c} \right) \left(1 + \frac{D_b}{D_c} \frac{\partial b}{\partial c} \right) \left(\frac{dc}{d\xi} \right)^2 d\xi \right)^{-1} \tag{4.7}$$

with $\partial b/\partial c = b_t K/(c(\xi) + K)^2$, is used to double check the results for the wave speed. Overall, we estimate that the results we present below are accurate within 2%.

First, we consider the high excitability mode with varying buffer affinity for a fixed buffer diffusion coefficient. The low affinity limit Eq. (3.6) for one-variable models does not apply in the multivariable case; however, considering the wave speed at $K = 100\,\mu$M in the two-variable model as a low affinity limit, we obtain the results presented in Fig. 8, which are qualitatively similar to those for the one-variable models (Figs. 3a, 3b).

Next, we study how the wave speed will be affected by the high affinity buffers with various diffusion coefficients. Similar to the one-variable models, this effect strongly depends on the system excitability. Numerical results in Fig. 9 show the dependencies of the wave

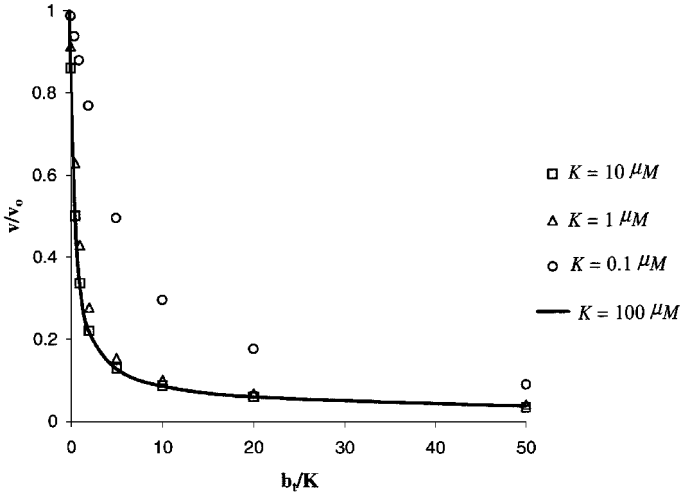

FIG. 8. Normalized wave speed vs buffer binding ratio for varying buffer affinity in the high excitability mode of the Li–Rinzel model ($D_b = 10\,\mu$m^2/s).

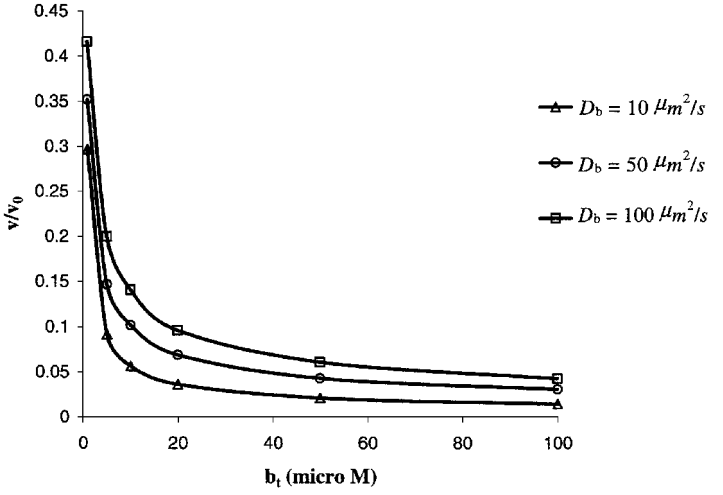

FIG. 9. Wave speed dependencies on the total concentration of a high affinity buffer ($K = 0.1\ \mu$M) at varying buffer diffusion coefficient in the high excitability mode of the Li–Rinzel model.

speed on the total buffer concentration at varying buffer diffusion coefficients in the high excitability mode. As in the one-variable models (compare to the two upper plots in Fig. 6 for the CP model), the wave speed increases with the buffer diffusion coefficient and will never become negative. As for the low excitability mode, referring to the numerical results in Fig. 10, we see that the wave speed decreases with the buffer diffusion coefficient at a fixed total buffer concentration. When the total buffer concentration exceeds a critical level, the wave speed becomes negative as in the one-variable models.

In this case, however, with increasing total buffer concentration, we observe a sudden drop of wave speed preceding the change in the wave direction (Fig. 10). For b_t fixed close to, and to the right of, the sharp transition, the wave speed gradually decreases in time

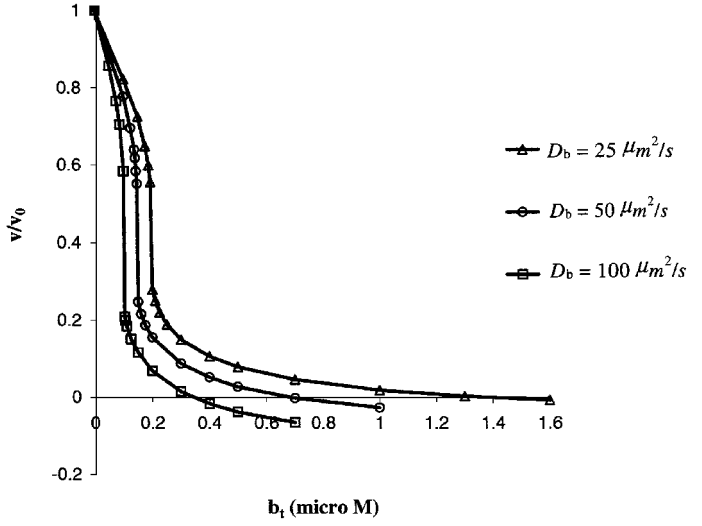

FIG. 10. Wave speed dependencies on the total concentration of a high affinity buffer ($K = 0.1\ \mu$M) at varying buffer diffusion coefficient in the low excitability mode of the Li–Rinzel model.

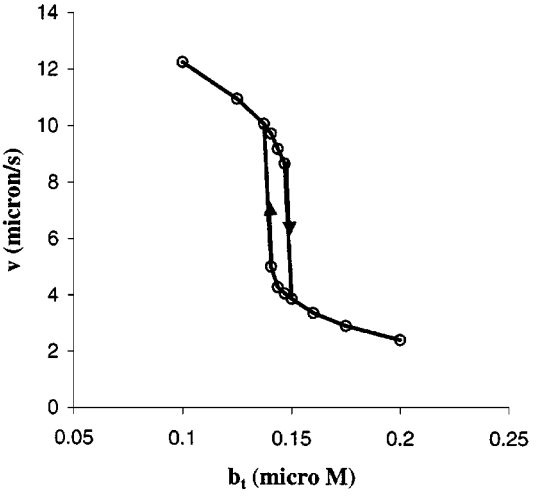

FIG. 11. Hysteresis loop in the wave speed dependence on the total buffer concentration in the low excitability mode of the Li–Rinzel model, at $K = 0.1\,\mu$M and $D_b = 50\,\mu\text{m}^2/\text{s}$.

from high to low values while the wave is settling in its stable profile. Thus, there is a finite interval of wave speed values for which no stable traveling wave exists. If we start with a wave profile, corresponding to a high total buffer concentration, and then gradually decrease the buffer concentration in our numerics, the jump occurs at a lower critical value. Thus, we observe a typical hysteresis loop presented in Fig. 11, which can be regarded as a magnified picture of the middle curve in Fig. 10 near its discontinuous jump. Thus, for a fixed buffer diffusion coefficient, there are at least two stable traveling waves with very different velocities when the total buffer concentration lies in a certain interval. Since we use an initial value problem solver to track down a traveling wave, only stable traveling waves are accounted for in Figs. 10 and 11. We expect the full picture to be a reverse $S-$curve as depicted in Fig. 12, with bifurcation occurring when we cross the limit points A_1 and

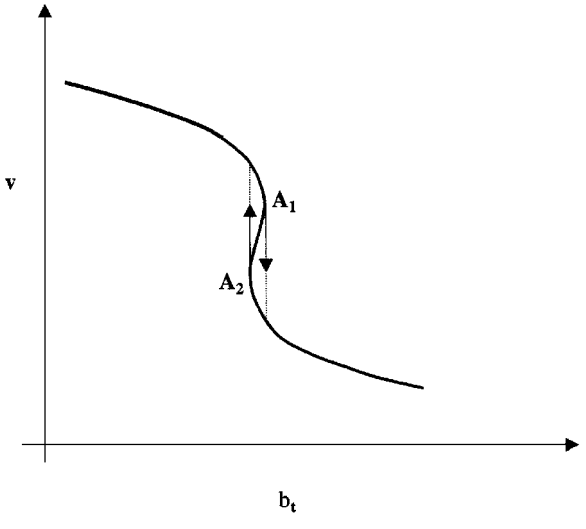

FIG. 12. A full reverse S-curve with the unstable branch A_1A_2.

A_2. Because the middle branch in the reverse $S-$curve usually corresponds to the unstable traveling waves, a continuation algorithm [27] has to be employed to trace the full response curve.

When the total buffer concentration is such that there are two stable traveling waves, each of the two stable branches has its own domain of attraction. Initial conditions that are close to one of the stable wave profiles will usually be attracted to it. If we push the total buffer concentration beyond the limit points (say, we start with the wave that belongs to the fast branch and then increase the buffer concentration to the value for which there exists only one stable wave on the slow branch), since now there is only one stable traveling wave, a large change in the wave speed has to take place to settle down into the stable wave profile. Such a discontinuous change is a hallmark of a bifurcation taking place in the system. No similar phenomenon has been observed in the one-variable models.

Finally, we note that as in the one-variable models, the wave speed decreases with the total buffer concentration.

5. THE 3D SIMULATIONS OF FERTILIZATION CALCIUM WAVES

It was recently suggested [15] that bistability is essential for the fertilization calcium waves experimentally observed in eggs after sperm fusion [28]. The calcium dynamics in living cells is visualized by injecting a fluorescent indicator that has calcium binding sites. When calcium binds to a binding site, it modifies fluorescent properties of the indicator, and the recorded changes in fluorescence closely follow the dynamics of the indicator bound form. Thus, a fluorescent indicator acts as a calcium buffer, in addition to the endogenous buffers (the proteins with calcium binding sites) that are always present in a cell. The fluorescent indicators usually used in biological experiments (e.g., fura-2 and Calcium Green [29]) have properties of fast, high affinity mobile buffers, and, as we saw in the previous sections, can significantly influence the properties of calcium waves. It is important to note that experimentally observed fertilization calcium waves are not traveling plane waves. They are transient processes initiated by a localized spike-like perturbation in a finite domain constrained by a cell membrane.

The Virtual Cell framework, within which we have developed the capability of treating fast reactions, allows us to run three-dimensional simulations using realistic geometry and realistic initial and boundary conditions. For example, our simulations of calcium waves in neuroblastoma cells [3, 4] use the geometry derived directly from experimental microscope images. In this section, we simulate fertilization calcium waves in a spherical cell (an egg) with a diameter of $50\,\mu$m using the Li–Rinzel model (see Eqs. (4.1)). A physiologically reasonable set of parameters given in Table III provides system bistability in the high excitability mode. We introduce two types of buffers in our 3D simulations. The immobile low affinity buffer, with a dissociation constant $K_1 = 10\,\mu$M and a total concentration $b_{t,1} = 200\,\mu$M, represents endogenous buffers, while the mobile high affinity buffer, with a diffusion coefficient $D_b = 50\,\mu\text{m}^2/\text{s}$ and a dissociation constant $K_2 = 0.24\,\mu$M, mimics fura-2. We will vary the total concentration $b_{t,2}$ of the mobile buffer in our numerical experiments. Let b_1 and b_2 be the concentrations of the bound forms of the endogenous buffer and the fluorescent indicator, respectively. With c and h as defined in the previous

TABLE III
Parameter Values Used for the Li–Rinzel Model in 3D Simulations of the Fertilization Calcium Waves

Parameter	Units	Value
J_0	μM s^{-1}	1000
d_{act}	μM	0.7
d_{inh}	μM	0.6
k_{on}	$(\mu\text{M})^{-1}$ s^{-1}	2.0
V_m	μM s^{-1}	10
K_p	μM	0.25
L	μM s^{-1}	1.51×10^{-2}
$b_{t,1}$	μM	200
K_1	μM	10
K_2	μM	0.24
D_c	$(\mu\text{m})^2$ s^{-1}	220

section, the governing set of equations is

$$\begin{aligned} \frac{\partial c}{\partial t} &= D_c \nabla^2 c + f(c,h) + R_1 + R_2, \\ \frac{\partial h}{\partial t} &= g(c,h), \\ \frac{\partial b_1}{\partial t} &= -R_1, \\ \frac{\partial b_2}{\partial t} &= D_b \nabla^2 b_2 - R_2, \end{aligned} \tag{5.1}$$

with $R_1 = -k_{on,1}(b_{t,1} - b_1)c + k_{off,1}b_1$ and $R_2 = -k_{on,2}(b_{t,2} - b_2)c + k_{off,2}b_2$. Here $k_{on,1}$, $k_{on,2}$, $k_{off,1}$, and $k_{off,2}$ are the buffering kinetic constants. Assuming fast buffering, we apply our approach and perform time splitting and pseudo-steady approximation. After that, the system (5.1) reduces to a "slow" subsystem,

$$\begin{aligned} \frac{\partial c}{\partial t} &= D_c \nabla^2 c + f(c,h), \\ \frac{\partial h}{\partial t} &= g(c,h), \\ \frac{\partial b_2}{\partial t} &= D_b \nabla^2 b_2, \end{aligned} \tag{5.2}$$

a "fast" subsystem, consisting of a "fast" invariant (see (2.6)),

$$c + b_1 + b_2 = I, \tag{5.3}$$

and a set of nonlinear algebraic equations,

$$\begin{aligned} c(b_{t,1} - b_1) &= K_1 b_1, \\ c(b_{t,2} - b_2) &= K_2 b_2, \end{aligned} \tag{5.4}$$

where $K_i \equiv k_{off,i}/k_{on,i}$, $i = 1, 2$. We then numerically solve Eqs. (5.2)–(5.4) using our two-step algorithm as described in Section 2.

We initiate a wave by a calcium spike localized near the cell membrane. The spike is centered at the membrane and has a radius of 5 μm and an amplitude of 30 μM. The initial conditions for h are determined as in the previous section. Both buffers are initially in equilibrium with calcium. Assuming that the calcium fluxes across the cell membrane can be ignored in this problem (see discussion in [15]), we use the zero flux boundary conditions. To reduce the time of computation, we take advantage of the rotational symmetry in the problem and perform calculations only in a quarter of the sphere. The discretization that we employ is $\Delta x = \Delta y = \Delta z = 0.65\,\mu$m (this mesh size results in 136,161 mesh points) and $\Delta t = 0.001$ s. We estimate that the results are accurate to within 5%.

We run simulations with varying total concentrations $b_{t,2}$. The results show a strong effect of the fluorescent indicator on wave formation. The indicator (the mobile buffer) usually causes a delay in the wave formation and can even prevent a wave if the total concentration

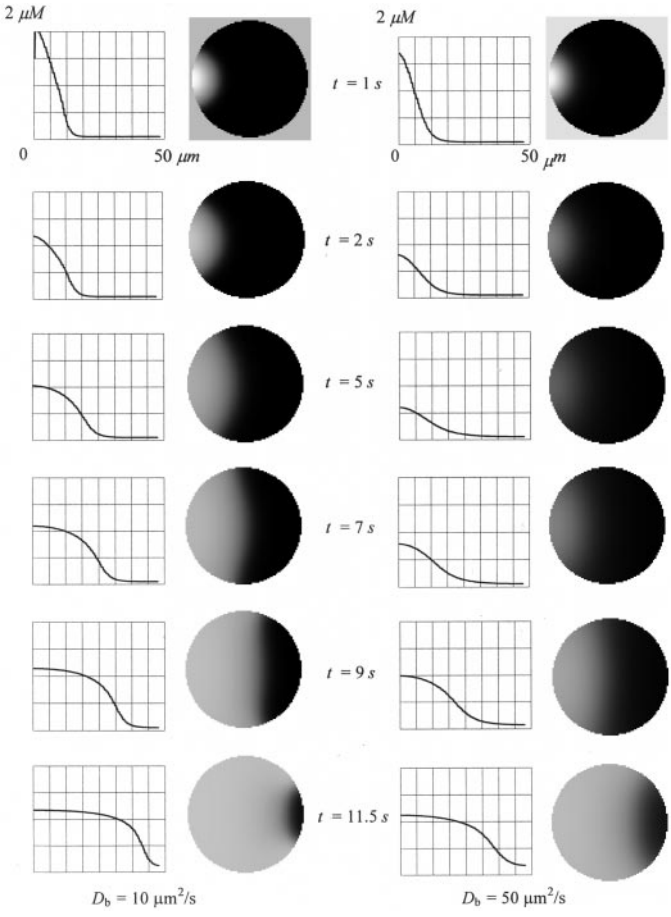

FIG. 13. Simulation of a fertilization calcium wave in the presence of a (9.5 μM) high affinity indicator ($K = 0.24\,\mu$M) for two different values of the indicator diffusion coefficient, $D_b = 10\,\mu$m^2/s (left column) and $D_b = 50\,\mu$m^2/s (right column). Images of the equatorial slice of an egg are accompanied with a line scan along the cell diameter that coincides with the symmetry axis. Fertilization is initiated at the left pole of the sphere.

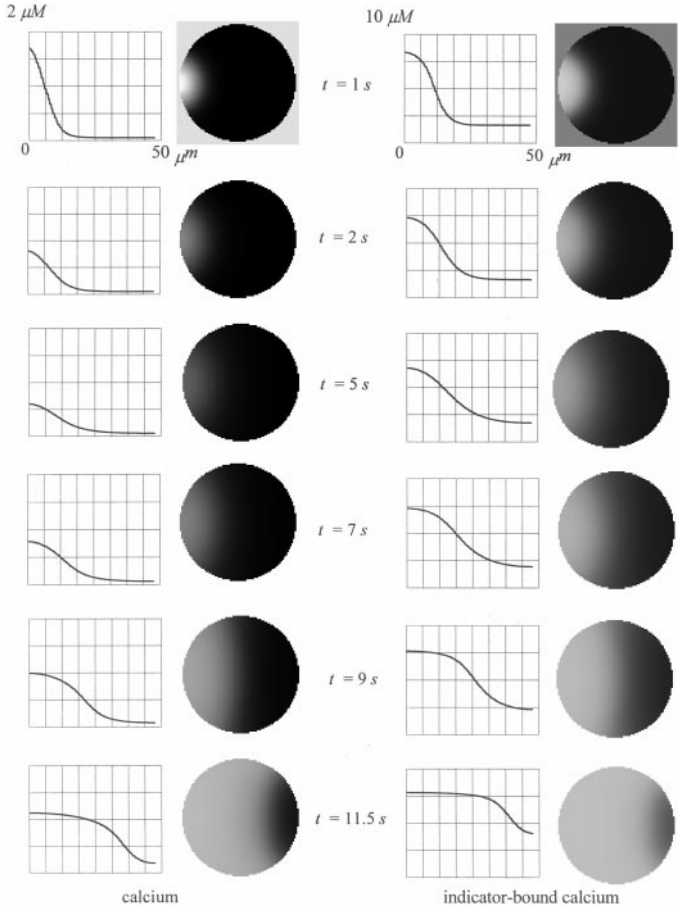

FIG. 14. Calcium wave in the presence of the fluorescent indicator fura-2 ($K = 0.24\,\mu$M, $D_b = 50\,\mu$m^2/s, and $b_t = 9.5\,\mu$M) (left column), as compared to the dynamics of the indicator-bound calcium that mimics the behavior of the fluorescence intensity (right column). Images of the equatorial slice of an egg are accompanied with a line scan along the cell diameter that coincides with the symmetry axis. Fertilization is initiated at the left pole of the sphere.

of a mobile buffer rises above a certain threshold for the given initial conditions. For our parameter set, this critical concentration is found to be approximately 11 μM.

We next fix the total concentration of the mobile buffer at $b_{t,2} = 9.5\,\mu$M and simulate wave propagation at two different buffer diffusion coefficients. The simulation results are presented in Fig. 13. It shows that the buffer with a higher diffusion coefficient causes a significant delay in wave formation. However, once initiated, the wave propagates faster with the higher buffer diffusion coefficient, in agreement with the results for traveling waves in systems with high excitability. Thus, when comparing the effect of buffers with different diffusion coefficients, we note two opposite roles a mobile buffer plays in wave propagation in the system with high excitability. The buffer with a higher diffusion coefficient slows down the process of wave formation, but then after a wave has been formed, makes it propagate faster. Overall, in the case of a small cell size, it takes longer for a wave to propagate throughout the cell in the presence of a more diffusive buffer even in the mode of high excitability.

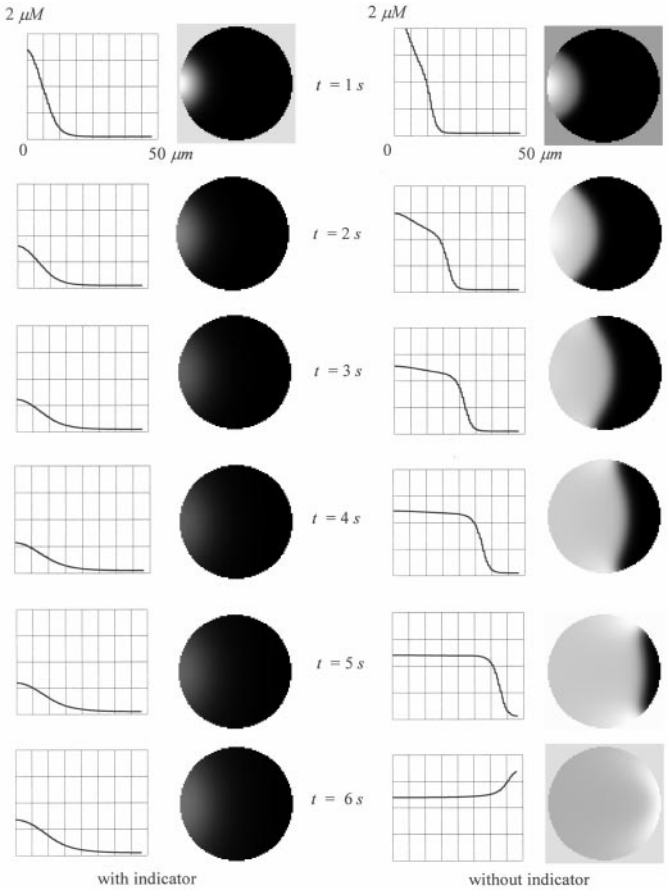

FIG. 15. Simulation of a fertilization calcium wave in the presence of fura-2 ($K = 0.24\,\mu$M, $D_b = 50\,\mu$m^2/s, and $b_t = 9.5\,\mu$M) (left column), and in the absence of a fluorescent indicator (right column). Images of the equatorial slice of an egg are accompanied with a line scan along the cell diameter that coincides with the symmetry axis. Fertilization is initiated at the left pole of the sphere.

In biological experiments, one directly measures the fluorescence intensity which correlates well with the bound buffer dynamics. In Fig. 14 we compare the dynamics of the bound form of fura-2 (which will be close to that of fluorescence intensity) with the actual dynamics of free calcium in the presence of the indicator. It illustrates a nonlinear relationship between the two dynamics. Thus, care has to be exercised in extracting the calcium dynamics from the experimentally measured fluorescence intensity [30].

Finally, the calcium waves in the presence of a moderate amount of fura-2 and without it are compared in Fig. 15. The fluorescent indicator strongly interacts with the initiating spike and substantially slows down the wave. Thus, even if the calcium dynamics is correctly extracted from the fluorescent intensity, it can still differ significantly from the actual situation without an indicator.

CONCLUSIONS

We have developed within the Virtual Cell framework a general numerical algorithm that performs a pseudo-steady approximation for multicomponent reaction-diffusion systems

containing fast and slow processes. The algorithm is based on time splitting and uses stoichiometry analysis of the reaction network.

The application of the algorithm to studying the effect of calcium buffering on calcium waves in bistable systems indicates that this effect can be drastically different depending on the buffer affinity and the system excitability. In systems with low excitability, the mobile buffers can stop the traveling wave and even reverse its direction, i.e., cause it to become self-annihilating, from the physiological point of view. In a more realistic two-variable model, the change in the wave direction can be preceded by a discontinuous transition (bifurcation) from states with fast traveling waves to states with slow ones, as the total buffer concentration increases. For some interval of parameter values, there may exist two stable traveling waves with very different velocities.

Three-dimensional simulations using realistic geometry and initial conditions show a strong effect of a fluorescent indicator on fertilization calcium waves. A more diffusive buffer causes a longer delay in wave formation and, at sufficient concentration, can prevent a wave. However, once a wave is initiated, it travels faster in the presence of a more diffusive buffer in a system with high excitability.

APPENDIX A

In this appendix, we prove that the solution to Eqs. (2.6) and (2.8) is independent of the choice of the matrix A, so long as its last $n-r$ columns are composed of $\{\mathbf{l}_1, \ldots, \mathbf{l}_{n-r}\}$ and it is non-singular.

Let A_1 and A_2 be two different choices of the non-singular matrix A. After pseudo-steady approximation, we have Eqs. (2.6) and (2.8). These are equivalent to the system

$$B A_i^T \frac{\partial \mathbf{u}}{\partial t} = A_i^T \alpha^{(f)} \vec{\nu}, \qquad i = 1, 2, \tag{A.1}$$

where the $n \times n$ matrix B is given by

$$B \equiv \begin{pmatrix} 0 & 0 \\ 0 & I_{n-r} \end{pmatrix}. \tag{A.2}$$

Here the I_{n-r} is the $(n-r) \times (n-r)$ identity matrix, and different zeros represent different zero matrices of suitable dimensions.

Since the last $n-r$ columns of A_i have to be $\{\mathbf{l}_1, \ldots, \mathbf{l}_{n-r}\}$, there exists a $n \times n$ matrix

$$C \equiv \begin{pmatrix} C_1 & 0 \\ C_2 & I_{n-r} \end{pmatrix} \tag{A.3}$$

with C_1 and C_2 being suitable sized matrices, such that

$$A_2 = A_1 C. \tag{A.4}$$

Because both A_1 and A_2 are non-singular, C has to be non-singular. This makes C_1 a non-singular $r \times r$ matrix. It is then easy to check that

$$C^{-1} = \begin{pmatrix} C_1^{-1} & 0 \\ -C_2 C_1^{-1} & I_{n-r} \end{pmatrix}. \tag{A.5}$$

Now using Eqs. (A.1) for $i = 2$ and Eq. (A.4), we have

$$(C^T)^{-1} B C^T A_1^T \frac{\partial \mathbf{u}}{\partial t} = A_1^T \alpha^{(f)} \vec{v}. \tag{A.6}$$

Note that $(C^T)^{-1} = (C^{-1})^T$. A simple calculation then shows that

$$(C^T)^{-1} B C^T = \begin{pmatrix} 0 & -C_2 C_1^{-1} \\ 0 & I_{n-r} \end{pmatrix}. \tag{A.7}$$

The last $(n - r)$ equations in (A.6) are equivalent to $\frac{\partial}{\partial t}(\mathbf{l}_i \cdot \mathbf{u}) = 0$, $i = 1, \ldots, n - r$. Thus there is no effect due to the matrix $C_2 C_1^{-1}$, and the left hand sides of the first r equations in (A.6) are zero. In other words, the solution of (A.1) for $i = 2$ is the same as the solution of (A.1) for $i = 1$. The proof is therefore complete.

APPENDIX B

In this appendix, we first derive Eq. (3.5) and then show that it reduces to Eq. (3.6) in the low buffer affinity limit.

In the absence of buffering, a one-variable bistable model is described by the equation

$$\frac{\partial c}{\partial t} = D_c \nabla^2 c + f(c), \tag{B.1}$$

which is a particular case of Eq. (1.1) with the function $f(c)$ having bistable properties as shown in Fig. 2a. Equation (B.1) is known to allow for the solutions of a traveling wave type $c(x + vt) = c(\xi)$ with a constant wave speed v [14, 21]. The wave shape therefore satisfies

$$v c_\xi = D_c c_{\xi\xi} + f(c), \tag{B.2}$$

and boundary conditions $c(-\infty) = C_{\min}$, $c(+\infty) = C_{\max}$. Multiplying Eq. (B.2) by c_ξ and integrating from $-\infty$ to $+\infty$, we derive a general expression for the wave speed

$$v = \left(\int_{C_{\min}}^{C_{\max}} f(c)\, dc \right) \left(\int_{-\infty}^{\infty} \left(\frac{dc}{d\xi} \right)^2 d\xi \right)^{-1}. \tag{B.3}$$

Simple dimensional analysis of Eq. (B.1) shows that if we scale the reaction term $f(c)$ by a factor of α the wave speed will change $\propto \alpha^{1/2}$. It then follows from Eq. (B.3) that the integral

$$\int_{-\infty}^{\infty} \left(\frac{dc}{d\xi} \right)^2 d\xi \tag{B.4}$$

will also change as $\alpha^{1/2}$. On the other hand, if we scale the whole right hand side of Eq. (B.1) by a factor of β then the wave speed changes $\propto \beta$ and the integral (B.4) remains unchanged.

In the presence of a mobile buffer the system is governed by Eqs. (1.3) with the same function f. According to [22, Theorem 2.1, p. 15], there exist monotone traveling wave solutions connecting two stable steady states and a unique wave speed. For solutions of

this type, $c(x+vt)=c(\xi)$, $b(x+vt)=b(\xi)$, their wave profiles are now governed by the equations

$$vc_\xi = D_c c_{\xi\xi} + f(c) + R, \tag{B.5}$$

$$vb_\xi = D_b b_{\xi\xi} - R. \tag{B.6}$$

For this case, one can also derive the general expression for the wave speed, somewhat analogous to Eq. (B.3). To do that, we sum up Eqs. (B.5) and (B.6) thus excluding R, and consider $b(\xi)=b(c(\xi))$ (we have used the symbol b for two different functions). Then

$$b_\xi = \frac{\partial b}{\partial c} c_\xi, \qquad b_{\xi\xi} = \frac{\partial}{\partial \xi}\left(\frac{\partial b}{\partial c} c_\xi\right), \tag{B.7}$$

and

$$v\left(1+\frac{\partial b}{\partial c}\right) c_\xi = D_c c_{\xi\xi} + D_b \frac{\partial}{\partial \xi}\left(\frac{\partial b}{\partial c} c_\xi\right) + f(c). \tag{B.8}$$

Multiplying Eq. (B.8) by c_ξ and integrating from $-\infty$ to $+\infty$, we obtain

$$\begin{aligned} v\int_{-\infty}^{+\infty}\left(1+\frac{\partial b}{\partial c}\right) c_\xi^2\, d\xi &= D_b \int_{-\infty}^{+\infty} \frac{\partial}{\partial \xi}\left(\frac{\partial b}{\partial c} c_\xi\right) d\xi + \int_{C_{\min}}^{C_{\max}} f(c)\, dc \\ &= -D_b \int_{-\infty}^{+\infty} \frac{\partial b}{\partial c} c_\xi c_{\xi\xi}\, d\xi + \int_{C_{\min}}^{C_{\max}} f(c)\, dc. \end{aligned} \tag{B.9}$$

Note that so far we have made no approximations. From now on we consider the case of fast buffering. This assumption has two consequences. First, on the "slow" time scale, one can consider a buffer to be in a rapid equilibrium with calcium at each spatial point [5]. We thus use a pseudo-steady approximation, $R=0$, to determine the function $b(c)$ from Eq. (1.3c), $b(c)=b_t c/(K+c)$, where the equilibrium constant $K=k_{off}/k_{on}$ characterizes the buffer affinity to calcium. We then find

$$\frac{\partial b}{\partial c} = \frac{b_t K}{(K+c)^2}. \tag{B.10}$$

Second, on the "fast" time scale, the buffer effect on calcium dynamics is due to the buffer reaction only, because diffusion is slow. Therefore, on this time scale we get $R=-vb_\xi$ from (B.6) and then find the instantaneous distribution of $c_{\xi\xi}$ from (B.5)

$$c_{\xi\xi} = \frac{v}{D_c}\left(1+\frac{\partial b}{\partial c}\right) c_\xi - \frac{f(c)}{D_c}. \tag{B.11}$$

Since the integrals in (B.9) can be treated either as integrals over time for some fixed spatial point (slow time scale) or, equivalently, as integrals over the spatial coordinate for some fixed time (fast time scale), we can use both Eq. (B.10) and Eq. (B.11). Substituting them in Eq. (B.9), we obtain Eq. (3.5) that gives a general expression for the wave speed at fast buffering. Equation (3.5) can be easily extended to the case of multiple buffers.

We now show that Eq. (3.5) reduces to Eq. (3.6) in the low affinity limit $K/C_{\max} \gg 1$. In this limit, it follows from Eq. (B.10) that $\partial b/\partial c$ becomes a constant: $\partial b/\partial c = b_t/K$. Then Eq. (B.8) reduces to

$$v\left(1+\frac{b_t}{K}\right)c_\xi = \left(D_c + D_b\frac{b_t}{K}\right)c_{\xi\xi} + f(c),$$

which is equivalent to modifying the reaction term in the initial equation (B.1) by the factor $\alpha = (1 + D_b b_t/D_c K)^{-1}$ and the entire right hand side of (B.1) by the factor $\beta = (1 + b_t/K)^{-1}(1 + D_b b_t/D_c K)$. Then, as we noted above, the integral (B.4) will change $\propto \alpha^{1/2}$,

$$\int_{-\infty}^{\infty} (c_\xi)^2\, d\xi = \left(1+\frac{D_b b_t}{D_c K}\right)^{-1/2} \int_{-\infty}^{\infty} (c_\xi)_0^2\, d\xi, \tag{B.12}$$

where zero index denotes the case of no buffering. Because in the low affinity limit all internal braces in Eq. (3.5) become constants, one can easily see that this equation reduces to Eq. (3.6), by taking into account Eqs. (B.12) and (B.3).

ACKNOWLEDGMENTS

We thank Leslie Loew, Leslie Greengard, and John Wagner for helpful discussions and Frank Morgan for technical assistance. Anne-Marie Hunter, during her summer internship, ran numerous simulations with the Virtual Cell and helped in collecting and processing data. We are pleased to acknowledge support from National Institutes of Health through grants from National Center for Research Resources (RR13186 and RR10081).

REFERENCES

1. J. Schaff, C. C. Fink, B. Slepchenko, J. H. Carson, and L. M. Loew, A general computational framework for modeling cellular structure and function, *Biophys. J.* **73**, 1135 (1997).
2. J. Schaff, B. M. Slepchenko, and L. M. Loew, Physiological modeling with the Virtual Cell framework, in *Methods in Enzymology*, edited by M. Johnson (Academic Press, San Diego, in press).
3. C. C. Fink, B. Slepchenko, I. I. Moraru, J. Schaff, J. Watras, and L. M. Loew, Morphological control of inositol-1,4,5-triphosphate-dependent signals, *J. Cell Biol.* **147**, 929 (1999).
4. C. C. Fink, B. Slepchenko, I. I. Moraru, J. Schaff, J. Watras, and L. M. Loew, An image-based model of calcium waves in differentiated neuroblastoma cells, *Biophys. J.*, in press.
5. J. Wagner and J. Keizer, Effects of rapid buffers on Ca^{2+} diffusion and Ca^{2+} oscillations, *Biophys. J.* **67**, 447 (1994).
6. N. N. Yanenko, *The Method of Fractional Steps* (Springer-Verlag, New York/Berlin, 1971).
7. J. P. Sørensen and W. E. Stewart, Structural analysis of multicomponent reaction models, *AIChE J.* **26**, 98 (1980).
8. C. Reder, Metabolic control theory: a structural approach, *J. Theor. Biol.* **135**, 175 (1988).
9. M. J. Berridge, Cell signalling through cytoplasmic calcium oscillations, in *Cell to Cell Signalling: From Experiments to Theoretical Models*, edited by A. Goldbeter (Academic Press, London, 1989), p. 449.
10. M. Terasaki, N. T. Slater, A. Fein, A. Schmidek, and T. S. Reese, A continuous cellular network of endoplasmic reticulum in cerebellar Purkinje neurons, *Proc. Natl. Acad. Sci. USA* **91**, 7510 (1994).
11. J. Sneyd, J. Keizer, and M. J. Sanderson, Mechanisms of calcium oscillations and waves: A quantitative analysis, *FASEB J.* **9**, 1463 (1995).
12. N. L. Allbritton, T. Meyer, and L. Stryer, Range of messenger action of calcium ion and inositol 1,4,5-triphosphate, *Science* **258**, 1812 (1992).

13. J. Sneyd, Calcium buffering and diffusion: On the resolution of an outstanding problem, *Biophys. J.* **67**, 4 (1994).
14. J. Keener and J. Sneyd, *Mathematical Physiology* (Springer-Verlag, New York, 1998), p. 268.
15. J. Wagner, Y.-X. Li, J. Pearson, and J. Keizer, Simulation of the fertilization Ca^{2+} calcium wave in *Xenopus laevis* eggs, *Biophys. J.* **75**, 2088 (1998).
16. J. Sneyd, P. Dale, and A. Duffy, Traveling waves in buffered systems: Applications to calcium waves, *SIAM J. Appl. Math.* **58**, 1178 (1998).
17. R. Kupferman, P. P. Mitra, P. C. Hohenberg, and S. S.-H. Wang, Analytical calculation of intracellular calcium wave characteristics, *Biophys. J.* **72**, 2430 (1997).
18. S.V. Patankar, *Numerical Heat Transfer and Fluid Flow* (Taylor & Francis, Washington, DC, 1980).
19. J. Gosling, B. Joy, and G. Steel, *The Java Language Specification* (Addison–Wesley, Reading, MA, 1997).
20. H. Cheng, W. J. Lederer, and M. B. Cannell, Calcium sparks: Elementary events underlying excitation-contraction coupling in heart muscle, *Science* **262**, 740 (1993).
21. P. Grindrod, *The Theory and Applications of Reaction Diffusion Equations: Patterns and Waves* (Oxford Univ. Press, London, 1996).
22. A. Volpert, V. Volpert, and V. Volpert, *Traveling Wave Solutions of Parabolic Systems*, Amer. Math. Soc. Transl. (Amer. Math. Soc., Providence, 1944).
23. J. Klingauf and E. Neher, Modeling buffered $Ca^{2}+$ diffusion near the membrane: Implications for secretion in neuroendocrine cells, *Biophys. J.* **72**, 674 (1997).
24. Y.-X. Li and J. Rinzel, Equations for $InsP_3$ receptor- mediated $[Ca^{2}+]_i$ oscillations derived from a detailed kinetic model: A Hodgkin–Huxley like formalism, *J. Theor. Biol.* **166**, 461 (1994).
25. Y.-X. Li, J. Rinzel, J. Keizer, and S. S. Stojikovic, Calcium oscillations in pituitary gonadotrophs—Comparison of experiment and theory, *Proc. Natl. Acad. Sci. USA* **91**, 9895 (1994).
26. G. De Young and J. Keizer, A single-pool inositol 1,4,5-triphosphate-receptor-based model for agonist-stimulated oscillations in $Ca^{2}+$ concentration, *Proc. Natl. Acad. Sci. USA* **89**, 9895 (1992).
27. H.B. Keller, *Lectures on Numerical Methods in Bifurcation Problems* (Springer-Verlag, New York/Berlin, 1986).
28. L. F. Jaffe, The role of calcium explosions, waves, and pulses in activating eggs, in *Biology of Fertilization*, edited by C. B. Metz and A. Monroy (Academic Press, Orlando, FL), Vol. 3, p. 127.
29. R. Nuccitelli (Ed.), *A Practical Guide to the Study of Calcium in Living Cells*, Methods in Cell Biology (Academic Press, San Diego, 1994), Vol. 40.
30. G. Grynkiewicz, M. Poenie, and R. Y. Tsien, A new generation of Ca^{2+} indicators with greatly improved fluorescence properties, *J. Biol. Chem.* **260**, 3440 (1985).